Cement and Concrete Research

The role of sodium and sulfate sources on the rheology and hydration of C3A polymorphs

--Manuscript Draft--

Manuscript Number:	CEMCON-D-21-00585R1
Article Type:	Research paper
Keywords:	cubic C3A; orthorhombic C3A; Calcium sulfate; hydration; rheology
Corresponding Author:	José S. Andrade Neto Universidade Federal do Rio Grande do Sul BRAZIL
First Author:	José S. Andrade Neto
Order of Authors:	José S. Andrade Neto
	Paulo R. de Matos
	Angeles G. De la Torre
	Carlos E. M. Campos
	Philippe J.P. Gleize
	Paulo J. M. Monteiro
	Ana Paula Kirchheim
Abstract:	The higher reactivity of orthorhombic C3A (ort-C3A) in sulfate-containing solutions, compared with cubic C3A (cb-C3A), was previously related to the differences in crystal structure or the sodium in the ort-C3A pore solution. We analyzed the hydration of cb-C3A (in water and NaOH solution) and Na-doped ort-C3A in the presence of gypsum and hemihydrate. Calorimetry, in-situ XRD, TGA, and rheological tests were conducted. NaOH accelerated the hydration of cb-C3A, but ort-C3A still presented higher ettringite formation rate and earlier sulfate depletion. Ort-C3A pastes showed 10-20 times higher viscosities and yield stresses. Replacing gypsum by hemihydrate increased the ettringite precipitation rate and anticipated the sulfate depletion of ort-C3A but did not significantly influence cb-C3A hydration. The crystallization of hemihydrate into gypsum resulted in early (<10 min) stiffing of all C3A-hemihydrate pastes. Overall, the higher reactivity of ort-C3A is related to differences in crystal structure rather than the sodium in the pore solution.
Suggested Reviewers:	Erich D. Rodriguez, Dr. Professor, Universidade Federal de Santa Maria erich.rodriguez@ufsm.br Professor Erich has a great experience on cement chemistry / cement hydration, including some important publications regarding cubic and orthorombic C3A hydration
	Sandro Torres, PhD Professor, Universidade Federal da Paraiba sandromardentorres@yahoo.co.uk Professor Sandro has a great experience on cement hydration and specially working with X-ray diffraction, which is a important result of the present paper.
	Maria Juenger, PhD Professor, The University of Texas at Austin mjuenger@mail.utexas.edu Professor Juenger has a great experience with cement chemistry/hydration, with very important publications.
	Guoqing Geng, PhD UC Berkeley: University of California Berkeley guoqing.geng@psi.ch Mr. Geng has several important publications dealing with C3A hydration.
	Roman Fediuk, PhD

	Professor, Far Eastern University roman44@yandex.ru Professor Fediuk is an advanced researcher on the field of cement-based materials
	Dengwu Jiao, PhD Post doc researcher, Ghent University: Universiteit Gent dengwu.jiao@ugent.be Dr Jiao published several works related to cement science and technology in high impact journals (e.g. 10.1016/j.conbuildmat.2019.07.316; 10.1016/j.cemconres.2020.106345; 10.3390/ma13225164)
Opposed Reviewers:	
Response to Reviewers:	

The role of sodium and sulfate sources on the rheology and hydration of C_3A polymorphs

José S. Andrade Neto[1,a*], Paulo R. de Matos[2,3,b], Angeles G. De la Torre[4,c], Carlos E. M. Campos[5,d], Philippe J.P. Gleize[3,e], Paulo J. M. Monteiro[6,f], and Ana Paula Kirchheim[1,g]

[1] Programa de Pós-Graduação em Engenharia Civil: Construção e Infraestrutura / Universidade Federal do Rio Grande do Sul (UFRGS) – Av. Osvaldo Aranha 99, Centro Histórico, 90035-190, Porto Alegre/RS, Brazil
[2] Universidade Federal de Santa Maria (UFSM).
[3] Departamento de Engenharia Civil, Universidade Federal de Santa Catarina (UFSC), Brasil
[4] Departamento de Química Inorgánica, Cristalografía y Mineralogía, Universidad de Malaga, Campus Teatinos s/n., 29071 Málaga, Spain
[5] Laboratório de Difração de raios-X, Departamento de Física, Universidade Federal de Santa Catarina (UFSC)
[6] Department of Civil and Environmental Engineering, University of California, Berkeley, CA 94720, USA

[a]jose.andrade@ufrgs.br, [b]paulo.matos@ufsm.br, [c]mgd@uma.es, [d]carlos.campos@ufsc.br, [e]p.gleize@ufsc.br, [f]monteiro@ce.berkeley.edu, [g]anapaula.k@ufrgs.br

*Corresponding author.

ABSTRACT

The higher reactivity of orthorhombic C_3A (ort-C_3A) in sulfate-containing solutions, compared with cubic C_3A (cb-C_3A), was previously related to the differences in crystal structure or the sodium in the ort-C_3A pore solution. We analyzed the hydration of cb-C_3A (in water and NaOH solution) and Na-doped ort-C_3A in the presence of gypsum and hemihydrate. Calorimetry, *in-situ* XRD, TGA, and rheological tests were conducted. NaOH accelerated the hydration of cb-C_3A, but ort-C_3A still presented higher ettringite formation rate and earlier sulfate depletion. Ort-C_3A pastes showed 10-20 times higher viscosities and yield stresses. Replacing gypsum by hemihydrate increased the ettringite precipitation rate and anticipated the sulfate depletion of ort-C_3A but did not significantly influence cb-C_3A hydration. The crystallization of hemihydrate into gypsum resulted in early (<10 min) stiffing of all C_3A-hemihydrate pastes. Overall, the higher reactivity of ort-C_3A is related to differences in crystal structure rather than the sodium in the pore solution.

Keywords: cubic C_3A; orthorhombic C_3A; Calcium sulfate; Hydration; Rheology.

1 INTRODUCTION

Despite its low amount in Portland cement (PC) -generally between 4 wt% and 10 wt%- the tricalcium aluminate ($Ca_3Al_2O_6$ or C_3A) greatly influences the workability, setting, and initial strength of concrete due to its high reactivity. Depending on the alkali content incorporated during clinker production (either from raw materials or fuel composition), C_3A can present different crystal structures. In the presence of sodium, Na^+ ions substitute Ca^{2+}, and another Na^+ ion occupies an otherwise vacant site in the center of $Al_6O_{18}^{18-}$ rings, resulting in solid solutions - $Na_{2x}Ca_{3-x}Al_2O_6$ [1]. The crystal structure of this solid solution depends on the amount of Na incorporated. According to Takeuchi et al. [2] and Taylor [3], cubic C_3A is stable when $0 < x < 0.10$, while cubic C_3A and orthorhombic co-exists when $0.10 < x$ 0.16. Orthorhombic is the only polymorph presented when $0.16 < x < 0.20$, while x values higher than 0.20 stabilizes the monoclinic form. However, different values are reported by other authors [4–7]. This discrepancy happens as the sodium content needed to stabilize orthorhombic C_3A depends on several parameters, such as the synthesis route, the sintering and cooling temperature, the sintering time, and the presence of other minor elements like Fe, Mg, Si, among others [4–7]. In commercial PC, cubic and orthorhombic C_3A are found alone or in combination, while the monoclinic C_3A is not observed [3,8].

Cubic C_3A (cb-C_3A) reacts almost instantly with water at room temperature, resulting in quick stiffing, making PC's most practical applications unfeasible [9,10]. Calcium sulfate (gypsum and/or anhydrite) is added to the clinker to control the C_3A hydration and allow the practical use of PC. In the presence of calcium sulfate, ettringite is formed in the first minutes, according to Eq. 1, and the reaction is then slowed down for some hours [11–13]. In limestone-free cements and in pure C_3A-calcium sulfate pastes, when all calcium sulfate is consumed, the ettringite becomes unstable and reacts with the remaining C_3A to form monosulfate (SO_4-AFm), according to Eq. 2 [11–13]. In turn, the presence of limestone stabilizes the ettringite and promote the formation of hemicarbonate and monocarbonate [14,15].

$$C_3A + 3C\bar{S}H_2 + 26H \rightarrow C_6A\bar{S}_3H_{32} \quad \text{(Eq. 1)}$$

$$2C_3A + C_6A\bar{S}_3H_{32} + 4H \rightarrow 3C_4A\bar{S}H_{12} \quad \text{(Eq. 2)}$$

Orthorhombic C_3A (ort-C_3A) reacts similarly to cb-C_3A, forming the same products in the absence and presence of calcium sulfate. However, the rate of reaction is entirely different. In the absence of calcium sulfate, ort-C_3A reacts more slowly than cb-C_3A [12,16,17]. In contrast, the presence of calcium sulfate is ineffective in retarding the ort-C_3A reaction, and therefore it reacts faster than the cubic polymorph in the presence of calcium sulfate [10,12,16–20].

Kirchheim et al. [12] evaluated the hydration of cubic and orthorhombic C_3A alone and with different gypsum contents using calorimetry and XRD. Their results show that an increase in the gypsum contents reduces the hydration rate of cubic C_3A while increases the hydration of ort-C_3A. Similar results were observed by Myers et al. [17] when evaluating the hydration of cubic and orthorhombic C_3A in the absence and the presence of gypsum by calorimetry, XRD, and ICP-OES, and by Cheung et al. [19] and Alonso and Puertas [20] who evaluated the hydration of cubic and orthorhombic C_3A pastes with gypsum by calorimetry. Stephan and Wistuba [16] analyzing the hydration of different C_3A solutions (alone and in the presence of $CaSO_4$) by calorimetry and FTIR, found out that the sodium-doping accelerated the hydration of C_3A in the mixtures with $CaSO_4$. Kirchheim et al. [18] observed by in-situ soft X-ray and ^{27}Al NMR that the orthorhombic C_3A hydrates faster and formed larger ettringite needles than the cubic one in the presence of gypsum. Kirchheim et al. [10] also observed by SEM that orthorhombic C_3A hydration in the presence of gypsum results in larger ettringite crystals compare with cubic C_3A-gypsum pastes. These authors [10] also evaluated the rheology in a plate-plate rheometer and observed that the orthorhombic C_3A-gypsum pastes have a higher storage modulus (*i.e.*, less fluidity) than the cubic C_3A-gypsum pastes. Furthermore, as followed by Dubina et al. [21], by evaluating the pre-hydration of cubic and orthorhombic C_3A alone and with hemihydrate through water vapor sorption, the orthorhombic polymorph presents a higher probability to undergo more pronounced pre-hydration during storage. In addition, orthorhombic C_3A also has a higher likelihood of carbonate during storage [22].

Recent studies [17,23–25] suggest that the retardation of cb-C_3A hydration in the presence of calcium sulfate is due to the adsorption of SO_4^{2-} ions and/or Ca–S ion pairs in the Al-rich leached layer formed with the cb-C_3A dissolution. However, still not clear yet why the calcium sulfate is ineffective to retard the ort-C_3A hydration. This might be related to the difference in the crystalline structure or to sodium in solution with ort-C_3A

dissolution. Ort-C_3A presents a higher solubility of the ring structures of $Al_6O_{18}^{18-}$ [17,26], which would impair the formation of the Al-rich leached layer on the C_3A particles and possibly affects its dissolution rate [12,17]. In turn, Stephan et al. [16] suggest that the greater reactivity of ort-C_3A is due to the presence of sodium ions, released in the dissolution of the ort-C_3A, which would destabilize the amorphous alumina layer where the Ca-S ion-pair complexes are adsorbed according to the recent theory [23]. Another factor that can occur in ort-C_3A pastes is the formation of the U-phase at the expense of monosulfate and ettringite as final precipitate [27–29]. This corresponds to a Na-substituted AFm phase formed in highly alkaline pastes, and the ort-C_3A can provide the sodium ions required for the formation of such phase. The presence of the U-phase was previously observed in C_3A-gypsum pastes hydrating in 0.25-1.00 M [27,30,31] of NaOH solutions and in PC hydrating in 2.0-4.5 M NaOH solutions [32]. According to Li et al. [28], the U-phase formation can appear only at high alkaline concentrations, but the pH range in which this phase is stable has not been reported yet, and further studies are necessary.

As previously mentioned, gypsum ($CaSO_4 \cdot 2H_2O$) and/or natural anhydrite ($CaSO_4$) are added to the clinker to control the C_3A reaction. However, depending on the temperature of the cement mill, gypsum may dehydrate into hemihydrate ($CaSO_4 \cdot 1/2H_2O$) and/or soluble anhydrite ($CaSO_4$) [33,34], which are much more soluble than gypsum and natural anhydrite. The higher solubility of calcium sulfate will increase the available sulfate ions in the solution during the first minutes/hours and influence the C_3A hydration [35]. Pourchet et al. [35] reported that at low SO_3/C_3A ratios, the gypsum replacement by hemihydrate accelerates the cb-C_3A, forming more ettringite in the first hours and anticipating the sulfate depletion. Zunino and Scrivener [36] studied the hydration process of pure C_3S-cb-C_3A mixtures with different amounts of gypsum and hemihydrate. The authors described that the hemihydrate anticipates the sulfate depletion point. Increasing the sulfate demand of the mix - i.e., a higher wt% SO_3 is necessary to obtain optimal mechanical performance for the mixtures with hemihydrate. However, at higher SO_3/C_3A ratios, using hemihydrate as the sulfate source results in a slower hydration rate of the cb-C_3A than when gypsum is used [35]. The reason for this behavior is not known yet, and further studies are necessary.

It is vital to have a correct balance between C_3A reactivity and sulfate solubility. On the one hand, if low soluble sulfates are used in cements with higher C_3A reactivities, it may have an insufficient amount of sulfate in solution, causing flash set due to the formation of OH-AFm or SO_4-AFm [33,37,38]. On the other hand, if a high soluble calcium sulfate (e.g., hemihydrate or soluble anhydrite) is used in cements with low C_3A reactivity, a "false set" may occur due to the formation of larger gypsum crystals deriving from the re-hydration of those sulfates [33,38,39]. This reaction can negatively affect the rheology of fresh concrete and impair its proper application. Despite the importance of the compatibility between C_3A and calcium sulfate source, to the best of the author's knowledge, there are no studies regarding the hydration of pure ort-C_3A in the presence of hemihydrate, except for the Dubina et al. [21] study, previously mentioned, that evaluated the pre-hydration of cubic and orthorhombic C_3A in the presence of hemihydrate.

The present study aims to determine, for the first time, if either the change in the crystalline structure or the presence of sodium ions in the solutions are responsible for the higher reactivity of ort-C_3A, in comparison with cb-C_3A, in the presence of calcium sulfate. Additionally, the effect of the type of calcium sulfate source (gypsum/hemihydrate) on the hydration and rheology of cubic and orthorhombic C_3A pastes was studied. Isothermal calorimetry (IC), *in-situ* X-ray diffractometry (*in-situ* XRD), thermogravimetry analysis (TGA), scanning electron microscopy (SEM), and rheological tests were conducted.

2 MATERIALS AND METHODS

2.1 Materials

Cubic C_3A (cb-C_3A, $3CaO.Al_2O_3$) and orthorhombic C_3A (ort-C_3A, $Na_{2x}Ca_{3-x}Al_2O_6$) were purchased from Mineral Research Processing Cie (France). Both materials were synthesized in the laboratory from a stoichiometric mixture of calcium carbonate ($CaCO_3$) and alumina (Al_2O_3). Sodium carbonate ($NaCO_3$) was used to stabilize the orthorhombic polymorph. The mixtures of reagents were calcinated twice at 1350°C for 2 hours in platinum crucibles. In an intermediate step, between the calcinations, the materials were ground to a fine powder.

High purity (>96 wt%) natural gypsum ($CaSO_4 \cdot 2H_2O$) and hemihydrate ($CaSO_4 \cdot 1/2H_2O$) were used as calcium sulfate sources. Hemihydrate was prepared by heating the gypsum at 100 °C for 48 hours.

Cb-C_3A, ort-C_3A, gypsum, and hemihydrate were characterized by X-ray diffractometry (XRD) using an X´Pert MPD PRO diffractometer from PANalytical (Almelo, Netherlands) placed at Servicios Centrales de Apoyo a la Investigación (SCAI) at the University of Malaga (UMA, Spain). Monochromatic Cu-Kα_1 radiation, λ = 1.54059 Å, obtained by a Ge (111) monochromator and X'Celerator detector were used. The X-ray tube operated at 45 kV and 40 mA, and the samples were measured between 5º to 70º (2θ) with a step size of 0.0167° 2θ, using a spinning sample-holder (16 rpm) to enhance particle statistics. The crystalline phases of the raw materials were identified using the X'Pert Highscore software (PANalytical) and quantified by the Rietveld method using the GSAS II software. The fitting process was adjusted to obtain an R_{WP} lower than 15% and a goodness-of-fit ($GOF = R_{WP}/R_{exp}$) lower than 4. Figures 1 and 2 present the XRD patterns, and Table 1 shows the XRD-Rietveld results of both C_3A samples and the sulfate sources.

Table 1 – ICSD collection codes and XRD-Rietveld results (in weight percentages) of the raw materials.

Phase	**Chemical composition**	**ICSD**	**cb-C_3A**	**ort-C_3A**	**Gypsum**	**Hemihydrate**
Cubic C_3A	$Ca_3Al_2O_6$	1841	96.9	5.6	-	-
Orthorhombic C_3A	$Na_{2x}Ca_{3-x}Al_2O_6$	1880	-	94.4	-	-
Mayenite	$Ca_{12}Al_{14}O_{33}$	261589	2.0	-	-	-
Lime	CaO	75786	1.1	-	-	-
Gypsum	$CaSO_4 \cdot 2H_2O$	151692	-	-	96.1	-
Hemihydrate	$CaSO_4 \cdot 1/2H_2O$	69060	-	-	-	97.2
Dolomite	$CaMg(CO_3)_2$	66333	-	-	3.4	2.4
Quartz	SiO_2	200721	-		0.5	0.4
	R_{WP}/%		13.3	14.7	11.7	11.3
	GOF		3.1	4.1	3.1	2.7

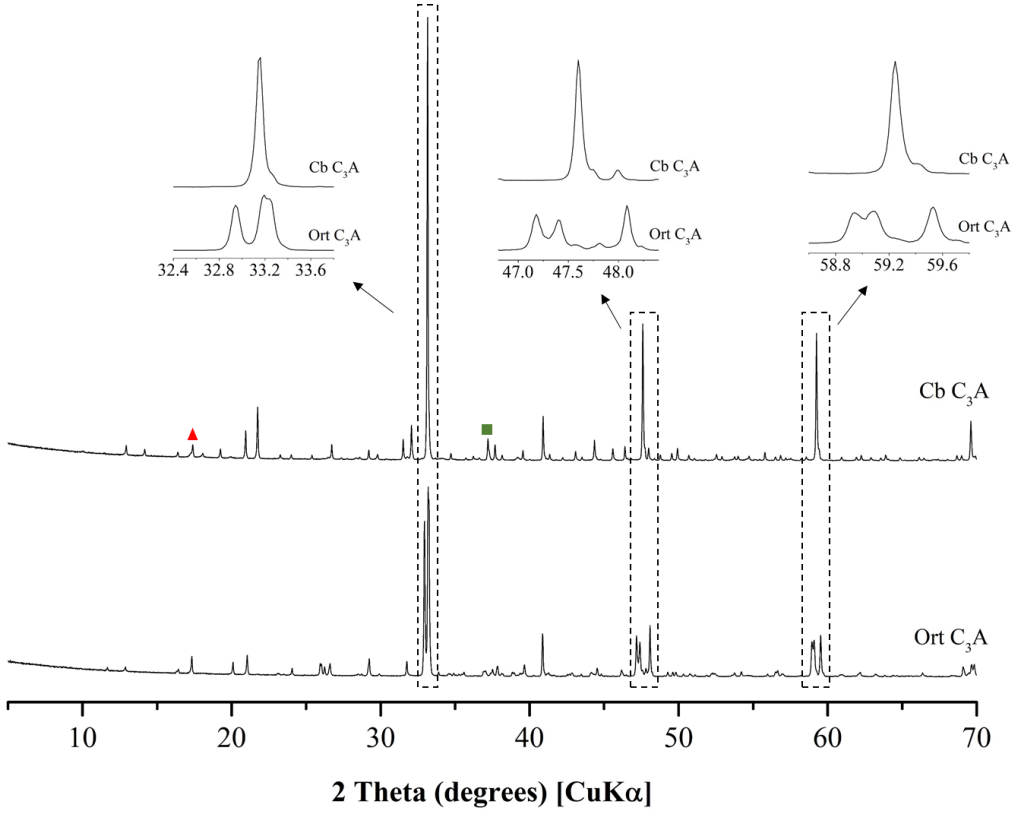

Figure 1 – XRD patterns for the cubic and orthorhombic C_3A. The non-labeled peaks correspond to C_3A reflections, while symbols indicate the main reflections of the minor phases. Triangle: Mayenite; Square: Lime. Note that in some cases, the peaks overlap with the peak of the main phases.

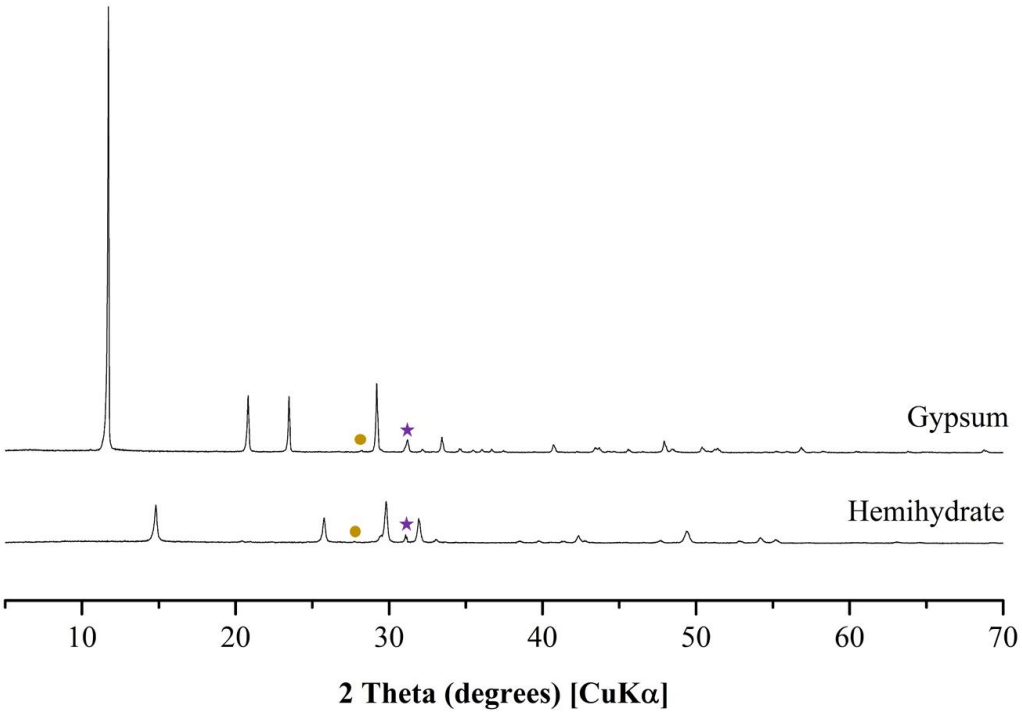

Figure 2 – XRD patterns for gypsum and hemihydrate. The non-labeled peaks correspond to gypsum or bassanite (crystalline hemihydrate) reflections, while symbols indicate the main reflections of the minor phases. Circle: Quartz; Star: Dolomite. Note that in some cases, the peaks overlap with the peak of the main phases.

The BET surface area of the raw materials was determined using ASAP 2420 equipment from Micromeritics (Georgia, USA), according to the guidelines presented by Palacios et al. [40]. The density was determined in an AccuPyc II 1340 pycnometer from Micromeritics (Georgia, USA), both equipment placed at SCAI at UMA. The particle size distribution was determined through laser diffraction, using PSA 1090 equipment from Anton Paar (Graz, Austria), with isopropanol as the dispersant, and considering Mie theory [40]. Table 2 presents the results of the physical characterization of the raw materials, and Figure 3 shows their particle size distribution. Both C_3As presented similar physical characteristics, with an equivalent median diameter and comparable BET surface area (difference of only 0.29 m^2/g, which maybe within the error of the method). Gypsum and hemihydrate presented similar particle size distribution and BET surface area as expected.

Table 2 – Physical characterization of the raw materials.

Property	**cb-C_3A**	**ort-C_3A**	**Gypsum**	**Hemihydrate**
BET surface area (m^2/g)	1.42	1.13	1.33	1.38
D_v 90 (μm)	30.8	28.7	51.8	40.8
D_v 50 (μm)	7.5	7.6	16.9	14.8
D_v 10 (μm)	1.6	1.8	3.6	3.5
Density (kg/m^3)	2940	2990	2350	--

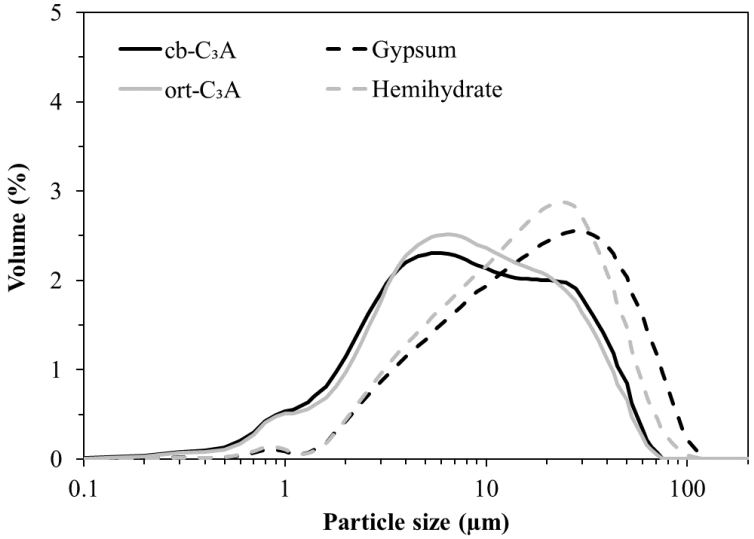

Figure 3 – Particle size distribution of the raw materials.

Table 3 presents the chemical composition of cb-C_3A, ort-C_3A, and gypsum, obtained by X-ray fluorescence (XRF), using an ADVANT'XP+ spectrometer from Thermo Fisher Scientific (Waltham, USA), placed at SCAI at UMA. For this test, the samples using fusion to form fused beads, providing a homogeneous representation of the sample. Cb-C_3A and ort-C_3A presented LOI of 2.76% and 2.20%, respectively, which probably is due to the absorption of water on their surface and slightly pre-hydration during grinding and storage as discussed by Dubina et al. [21].

Table 3 – Chemical composition, obtained by XRF, of the raw materials, expressed as the weight percentage of oxides. Loss on ignition (LOI) is also included.

Constituent	**cb-C_3A**	**ort-C_3A**	**Gypsum**
CaO	60.89	56.58	34.04
Al_2O_3	35.52	36.70	0.09
Na_2O	0.03	3.98	-
SiO_2	0.43	0.18	0.95
Fe_2O_3	0.08	0.06	0.16
MgO	0.11	0.09	0.81
SO_3	0.02	0.03	46.05
LOI	2.76	2.20	17.53

The amount of Na^+ released in ort-C_3A dissolution was quantified by inductively coupled plasma atomic emission spectroscopy (ICP-OES), using an Optima 7300DV spectrometry from Perkin Elmer (Massachusetts, USA). A release of 3.5 wt% of Na^+ (or 4.7 wt% of Na_2O) was observed with the dissolution of ort-C_3A in water, and this information was used for mix design (Section 2.2.1). This value is slightly higher than the value obtained by XRF (3.98 wt%), and this can be attributed to the inherent deviations on XRF tests.

2.2 Methods

2.2.1 Formulations and sample preparation

Table 4 shows the different formulations studied. Mixes with cb-C_3A, cb-C_3A + NaOH, and ort-C_3A were produced with gypsum or hemihydrate. For the mixes with cb-C_3A and ort-C_3A, distilled water was used, while for those with Na-cb-C_3A, a 0.99 M NaOH

solution was used. The molarity of NaOH solution was chosen to maintain the amount of Na^+ released with the dissolution of ort-C_3A, as obtained by ICP-OES (3.5 wt% of Na^+). Furthermore, as the sodium is progressively liberated with the dissolution of ort-C_3A, while it is fully available from the beginning on the Na-cb-C_3A, it is interesting to study the impact of different NaOH molarities on cb-C_3A hydration. Thus, in addition to the 0.99 M, the hydration of cb-C_3A_GYP pastes at 0.24 M and 0.48 M of NaOH solutions was also evaluated (only by calorimetry). These correspond to 25% and 50% of the Na^+ released with the total dissolution of ort-C_3A.

A fixed SO_3/C_3A ratio of 0.293 by weight was used for all mixtures, resulting in a gypsum/C_3A ratio of 0.64 and a hemihydrate/C_3A ratio of 0.58. This ratio falls within the range of SO_3/C_3A ratio usually found in PC (considering a C_3A content of 8 wt% and an SO_3 content of 2.3 wt.%), and similar ratios were used in several studies with C_3A-gypsum pastes [10–12,41]. The water/solid ratio was fixed at 1.00 by weight since it is the most common ratio used for C_3A pastes in literature [11,13,25,41], being enough to fully hydrate the C_3A and promote adequate workability. The w/s ratio used here does not consider the chemical bound water present in gypsum and hemihydrate, as it will not be available during mixing and the beginning of the reaction.

Table 4 – Formulations studied.

Mixture	C_3A (wt%)	Gypsum (wt%)	Hemihydrate (wt%)	Solution	SO_3/C_3A	w/s
cb-C_3A_GYP	61.08	38.92	-	Distilled water	0.29	1.0
Na-cb-C_3A_GYP	61.08	38.92	-	0.99 M NaOH		
ort-C_3A_GYP	61.08	38.92	-	Distilled water		
cb-C_3A_HEM	64.22	-	35.78	Distilled water		
Na-cb-C_3A_HEM	64.22	-	35.78	0.99 M NaOH		
ort-C_3A_HEM	64.22	-	35.78	Distilled water		

The anhydrous materials (C_3A and gypsum/hemihydrate) were manually mixed for 10 minutes in an agate mortar. At room temperature, the 0.99 M NaOH solution was prepared by dissolving NaOH in distilled water by magnetic stirring for 30 minutes. As the NaOH dissolution is exothermic, the solutions were prepared at least 24 hours before mixing the

C_3A pastes to prevent the heat release in its dissolution from interfering with the C_3A hydration and the isothermal calorimetry results.

For the preparation of the C_3A pastes, 2 g of pre-mixed anhydrous materials (cb-C_3A/ort-C_3A and gypsum/hemihydrate) were placed in a 20 mL vessel. Then, the deionized water or the Na^+ water solutions was added, and the materials were mixed for 2 minutes using a rotational mixer at 350 rpm.

For the calorimetry analysis, the mixing procedure was conducted inside the 20 mL glass ampoule used for the isothermal calorimetry tests (see section 2.2.2), and the plastic rod was left inside the glass ampoule to minimize the loss of material during mixing. The mixing procedure and insertion of glass ampoule in the calorimetry were done in less than 3 minutes after the initial contact between water and C_3A. For the TGA, in-situ XRD, SEM, and rheological tests, the mixes were prepared in plastic vessels and then hermetically closed. For the TGA and SEM analysis, the paste remained inside the closed vessels until the hydration stoppage.

For the SEM analysis, the hydration of C_3A pastes was stopped at 30 and 120 minutes for the gypsum containing and at 10 minutes for the hemihydrate-containing samples. The hydration was stopped at 1 hour, 1, 2, and 3 days for the TGA analysis. About 1 g of each paste was mixed with 50 ml of isopropanol for 30 minutes while stirring; due to the soft consistency of the pastes for up to 3 days, no grinding process was required. Then, the sample was filtered at a low vacuum through a nylon filter with a 15 µm opening for 10 minutes and dried in an oven at 40 °C for another 10 minutes. Finally, the sample was stored in a desiccator with silica gel and low vacuum until testing.

2.2.2 Isothermal calorimetry (IC)

For IC analyses, an eight-channel Thermal Activity Monitor of Tam Air, TA Instruments (New Castle, DE, USA) was used. The pastes were mixed ex-situ, but inside the glass ampoule, as described in item 2.2.1. Distilled water was used as reference material, and the amount of water used as reference was calculated according to Wadsö [42] to obtain the same heat capacity as the C_3A paste. The heat flow (thermal power, mW/g of solids) and the cumulative heat (integral of thermal power, J/g of solids) were recorded for up to 3 days at 20°C.

2.2.3 *In-situ X-ray diffraction (In-situ XRD)*

In-situ XRD was conducted up to 48 hours in an X`Pert Pro (PANalytical) diffractometer equipped with Soller and anti-scattering slits, 1/2^{o} fixed divergent slit set up, and X´Celerator detector. The diffractometer operated at 45 kV and 40 mA with CuKα radiation given a wavelength of 1.5418Å. The scanning range, step size, and counting time were respectively 7-55° 2θ, 0.0167° 2θ, and 24.765 sec/step, and the sample was rotated at 2 sec/rev to improve the statistics of data collection. Immediately after mixing, the fresh paste was placed on the sample holder and covered with a Kapton film to prevent water loss and carbonation. The measurements started 40 minutes after the first contact between the water and the dry materials; each scan took about 10 minutes, and three samples were tested alternatively, placed at X-ray beam automatically by a robotic arm, providing an XRD pattern for each sample every 30 minutes, totalizing about 90 measurements for each sample.

For XRD data analysis, TOPAS v.5 software was used. The U-phase was found in most pastes (discussed later in Section 3.2), which corresponds to a sodium-substituted AFm phase formed in highly alkaline cement pastes [27,29]. According to Ectors [43], the layered nature of AFm-type structures often results in stacking disorder and anisotropic peak broadening in XRD, making the crystal structure determination difficult. The lack of a well-defined crystal structure for this phase would make Rietveld quantitative phase analysis inaccurate. Thus, a semi-quantitative phase analysis (SQPA) was conducted as detailed next. The crystallographic information files used for phase identification are detailed in Table 5.

Table 5 – Crystallographic information files used for phase identification.

Phase	Reference code	Reference
C_3A cubic	1841*	Mondal and Jeffery [7]
C_3A orthorhombic	1880*	Nishi and Takeuchi [1]
Ettringite	155395*	Goetz-Neunhoeffer and Neubauer [44]
Gypsum	151692*	de la Torre et al. [45]
Hemihydrate	69060*	Bezou et al. [46]
U-phase	00-044-0272**	Post and Pollmann [47]

*ICSD code; **ICDD code.

2.2.3.1 Kapton film and free water fitting

In order to systematically account for the background contributions caused by the Kapton film and free water while avoiding manual background fitting (which highly depends on the operator), those were fitted using hkl phases. The Kapton film was first measured over a silicon single crystal, and the data were fitted with a Pawley range using the structural parameters proposed by Scherb et al. [48]: P4/mmm space group and lattice parameter a = 9.72 Å; c = 26.53 Å. The crystallite size (Lorentzian function) and hkl intensities were refined in this step. Subsequently, a corundum (α-Al_2O_3) sample covered with Kapton was measured, and the lattice parameters of the Kapton hkl phase were refined. This allowed placing the hkl phase along the 2θ axis correctly. For the free water model creation, corundum:water paste (in 50:50 wt%) covered with Kapton was measured. The lattice parameters, the crystallite size (Lorentzian function), and scale factor of corundum, the scale factor of the Kapton hkl phase, and the background (n=0 order Chebyshev) were refined in the pure corundum sample above-mentioned and fixed for the corundum:water sample (except for the scale factor of the corundum phase which was allowed to be refined). The diffuse scattering caused by the water was then fitter with a Pawley range using the space group P4/mmm. The lattice parameters, the crystallite size (Lorentzian function), and the hkl intensities of the free water model were refined and fixed. Figure 4 shows an example of a fitted *in-situ* diffractogram accounting for the contribution of both Kapton film and free water, in addition to the crystalline phases.

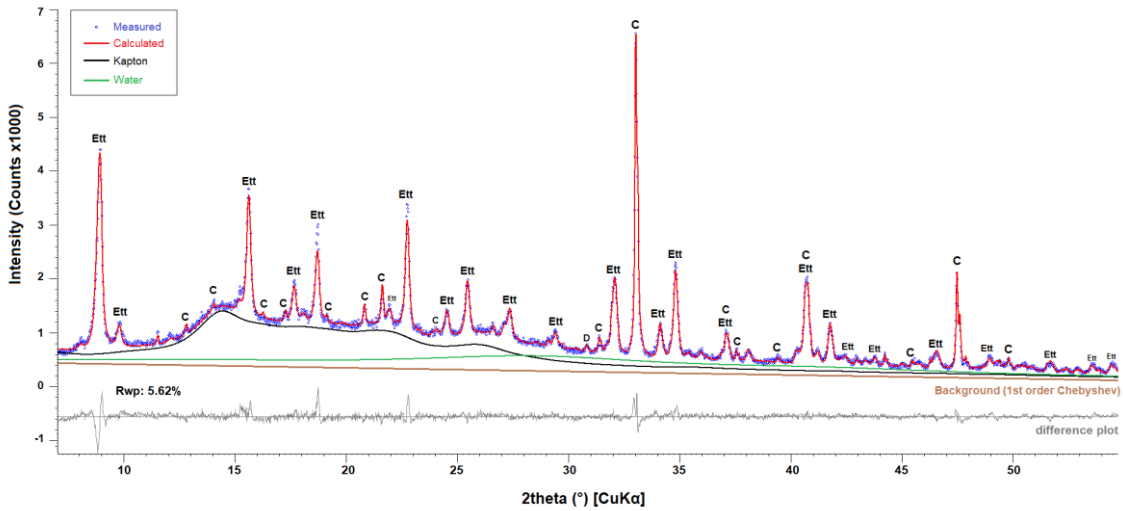

Figure 4 – Example of fitted XRD pattern of in-situ measurement for cb-C_3A_GYP paste at 48 hours of hydration. Ett: ettringite; C: C_3A (cubic); D: dolomite.

2.2.3.2 Semi-quantitative phase analysis (SQPA)

SQPA was conducted by determining the scale factor of each crystalline phase over time relative to its highest scale factor measured. Different qualitative or SQPA approaches based on peak intensities of XRD patterns were used to evaluate the cement paste hydration. Guo et al. [49], Gardner et al. [50], and Shunman et al. [51] analyzed absolute intensity values at given 2θ positions to assess the formation of hydrated phases (e.g., portlandite) in powder XRD. More elaborately, Quennoz and Scrivener [11,52] evaluated the area of a single representative peak for each phase over time for in situ XRD measurements, manually subtracting the background. However, relying on a single peak may provide misleading results since preferred orientation can occur, while the scale factor of the phases accounts for the whole XRD pattern. It is stressed that the weight fraction of a given crystalline phase is linearly proportional to its scale factor [53].

The global parameters refined were sample displacement (to account for height variations caused by paste expansion/shrinkage over time) and background (1st order Chebyshev polynomial). After including the Kapton and free water hkl phases (detailed in Section 2.3.3.1) in the refinement, the crystalline phases were included one by one. For the U-phase, a hkl phase was created using the space group, lattice parameters, and relative intensities of the ICDD 00-044-0272 file, detailed in the Supplementary Material (Table S1 and S2, Figure S1). The lattice parameters and peak shape (Thompson-Cox-Hastings pseudo-Voigt profile function [54]) of the anhydrous phases (i.e., C_3A, gypsum, and bassanite) were previously refined in dry samples and fixed for hydrating samples. The lattice parameters and peak shape of the hydrated phases (i.e., ettringite and U-phase) were refined for each mix using the XRD pattern that had the highest content of the respective phase and then were fixed for the other patterns. Pseudo-Voigt peak shape fitting instead of the fundamental parameters approach was chosen because it led to more stable refinements over time. The preferred orientation of gypsum (020), ettringite (010), and U-phase (003) were refined using the March-Dollase function [55] for accounting for crystal orientation on the surface of the Kapton film.

2.2.4 Thermogravimetry analysis (TGA)

TGA was performed in a TGA 2 analyzer from Mettler Toledo (Columbus, Ohio, USA). The samples (≈10 mg) were placed in open platinum crucibles under airflow. The temperature ranged between room temperature (RT) and 1000 °C with a heating rate of 10 °C/min. From the TGA results, the bound water content was determined. After

stopping hydration, the bound water content of the pastes was assigned to the weight loss from RT to 550°C. The actual bounded water can be calculated by Eq. 3 [56]:

$$BW = \frac{BW_{ATD} \cdot CM}{100 - BW_{ATD}} \quad \text{(Eq. 3)}$$

BW corresponds to actual chemically bound water content, BW_{ATD} is the mass loss measured up to 550ºC from TGA curves, and CM is the solid, i.e., C_3A-sulfate source content (all the numbers in weight percentages).

2.2.5 Scanning electron microscopy (SEM)

SEM images of the hydrated samples in dry powder form (detailed in Section 2.2.1) were recorded using a VEGA3 (TESCAN) microscope operating at 15 kV. A small portion of powder was placed over a carbon adhesive tape and coated with gold. Images were acquired at the ×5000-40000 range.

2.2.6 Rheological tests

The rheological tests were conducted on a Haake MARS III (Thermo Scientific) rheometer using a parallel plate geometry with 20 mm diameter and serrated surface. The axial gap was 1.000 mm, and the temperature was kept at 23.0 ± 0.1°C. The measurements started 10 minutes after the first contact between the water and the dry materials, and a shear cycle was recorded every 10 minutes until 120 minutes of hydration. An insulation hood was used to prevent water evaporation.

Firstly, the sample was pre-sheared at 100 s^{-1} for 30 seconds, followed by a 30-second rest. Subsequently, the shear rate was increased from 0.1 to 100 s^{-1} in 10 steps and then decreased back to 0.1 s^{-1} in the same steps. Each step took 10 seconds (which was confirmed to be enough to reach a steady-state flow) and the last 3 seconds were recorded. The decreasing portion of the flow curves was used to obtain the rheological properties of the paste. The yield stress was determined using the Casson model [57] (Eq. 4), as also used in several studies with cement pastes [58–60].

$$\sqrt{\tau} = \sqrt{\tau_0} + \sqrt{\mu_\infty} \cdot \sqrt{\dot{\gamma}} \quad \text{(Eq, 4)}$$

Where τ is the shear stress (in Pa), $\dot{\gamma}$ is the shear rate (in s^{-1}), τ_0 is the yield stress (in Pa), and μ_∞ is the viscosity (in Pa.s).

This model provided the best overall fit for the data, while the Herschel-Bulkley model (conventionally used to describe the pseudoplastic flow of cement pastes) provided unrealistic values, i.e., negative yield stress values or visible misfits. The Casson model only provides the viscosity at an infinite shear rate, and this has no practical meaning for cement-based materials, so it was used here only for comparison between the samples.

3 RESULTS

3.1 Isothermal Calorimetry

Figure 5 presents the heat flow, and cumulative heat curves of C_3A pastes with gypsum up to 90 hours. All pastes evaluated presented the typical heat flow curve profile of C_3A hydration, divided into three periods. In the first ~30 minutes of hydration, a great exothermic peak of heat release is observed, followed by a sharp reduction in the heat flow. According to Quennoz and Scrivener [11], this first heat release is related to the initial dissolution of C_3A and gypsum and the formation of the first ettringite and OH-AFm crystals. After the end of this great heat release, a low heat releasing period begins. Several hypotheses were proposed to explain the mechanism responsible for the occurrence of this period of low heat release, which is not observed in the C_3A hydration without calcium sulfate. The most accepted theory nowadays is that SO_4^{2-} ions and/or Ca–S ion-pair complexes are adsorbed on an Al-rich leached layer formed at the partially dissolved C_3A surface [17,23,61,62]. During the period of low heat release, the sulfates are being consumed due to ettringite formation. Finally, when all sulfate from the solution is consumed – known as sulfate depletion– a new exothermic peak is observed due to a new fast dissolution of C_3A and formation of AFm phases, as confirmed by XRD (see Section 3.2) and previously observed by Quennoz and Scrivener [11] and Kirchheim *et al.* [12].

As shown in Figures 5 and S2, the length of the period of low heat release and the intensity of the main heat flow peak were greatly influenced by the presence of sodium. The cb-C_3A_GYP sample exhibited a low (~ 6.5 mW/g of C_3A) and a broad main peak of heat release -between 25 and 70 h. The external addition of sodium in solution (i.e., incorporation of NaOH) anticipated and increased the main peak of heat release -which now occurred between 15 and 35 hours with a maximum value of ~ 27 mW/g of C_3A.

As observed in Figure S2, the amount of external sodium added (*i.e.*, varying the NaOH molarity) did not influence the beginning of the second peak, indicating that the amount of NaOH does not influence the moment of sulfate depletion occurrence. However, the greater the amount of sodium added (*i.e.*, the higher the NaOH molarity), the higher is the second peak: the sample hydrating at the 0.24 M presented a maximum of the second peak of ~ 12 mW/g of C_3A while the sample hydrating at 0.99 M of NaOH presented a maximum of ~ 27 mW/g of C_3A.

Finally, the reaction of ort-C_3A, which has Na^+ in its crystalline structure, was even faster, with most of the reaction occurring within the first 24 hours. Furthermore, ort-C_3A presented two peaks in the first 24 hours: the first peak is related to very fast ettringite precipitation and gypsum consumption, while the second is related to a new C_3A dissolution and AFm precipitation, as observed in the XRD results and discussed in Section 3.2. These results corroborate with previous studies [12,17,20], which observed a higher heat-releasing of ort-C_3A-GYP compared with cb-C_3A-GYP in the first hours of hydration.

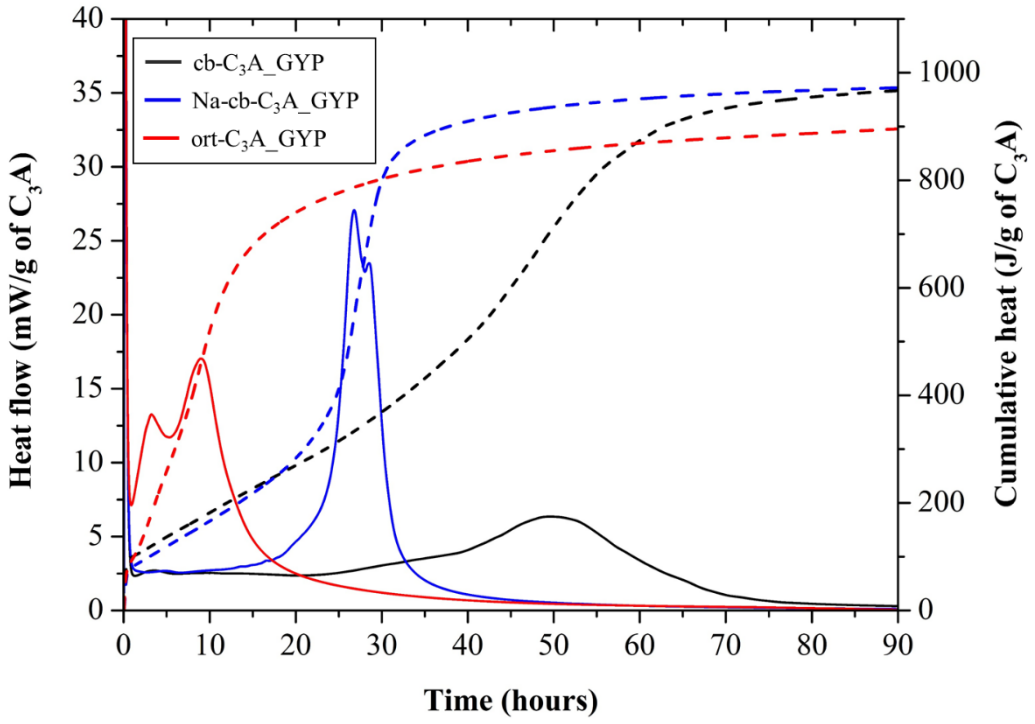

Figure 5 – Heat flow curves (solid lines and primary/left "y" axis) and cumulative heat curves (dashed lines and secondary/right "y" axis) of the C_3A pastes with gypsum during the first 90 hours of hydration.

Figure 6 presents the heat flow and cumulative heat curves of cb-C_3A, Na-cb-C_3A, and ort-C_3A with gypsum and hemihydrate. The replacement of gypsum with hemihydrate had different impacts on the hydration of C_3A polymorphs: it increased the heat released in the first hours in the ort-C_3A, retarded the second heat flow peak of the Na-cb-C_3A, while did not influence the heat flow and cumulative heat curves of the cb-C_3A.

Regarding the cb-C_3A (Figure 6a), the paste with hemihydrate presented a slightly broader and smaller peak – between 20 and 80 hours with a maximum value of ~ 4.7 mW/g of C_3A. Therefore, the calcium sulfate source did not have a great influence on the cb-C_3A hydration. In turn, the use of hemihydrate in Na-cb-C_3A (Figure 6b) delayed the main heat flow peak (by about 11 hours) but increased by approximately 30% compared to the gypsum samples. Pourchet et al. [35] observed that the replacement of gypsum with hemihydrate delayed the cb-C_3A reaction when more than 15wt.% of equivalent gypsum (related to the C_3A wt.%) was used, which corroborates with the behavior observed for the Na-cb-C_3A, but not for the cb-C_3A (this is later discussed in Section 4.2).

As for the ort-C_3A, the replacement of gypsum with hemihydrate increased the intensity of the heat flow peak, increasing the heat release within the first day (Figure 6c). Ort-C_3A_HEM hydration showed three heat release peaks between 30 minutes and 24 hours. These peaks are respectively related to hemihydrate conversion into gypsum, very fast ettringite precipitation, C_3A and gypsum dissolutions, and AFm precipitation, as further discussed in Section 3.2.

It is worth noting that all the mixes with hemihydrate presented a higher heat release within the first hour when compared with the respective mixes containing gypsum. This probably results from hemihydrate hydration and recrystallization in gypsum, which is exothermic and generally occurs in the first hour (as confirmed by XRD and SEM; see Sections 3.2 and 3.4). This hypothesis agrees with thermodynamic modeling (see Supplementary Materials, Figure S3), which showed that the use of hemihydrate instead of gypsum in the cb-C_3A paste is expected to increase the cumulative heat by 83 J/g of C_3A. This value is very close to the increase of 79.7 J/g of C_3A in the cumulative heat obtained by calorimetry at 90 hours when hemihydrate is used instead of gypsum.

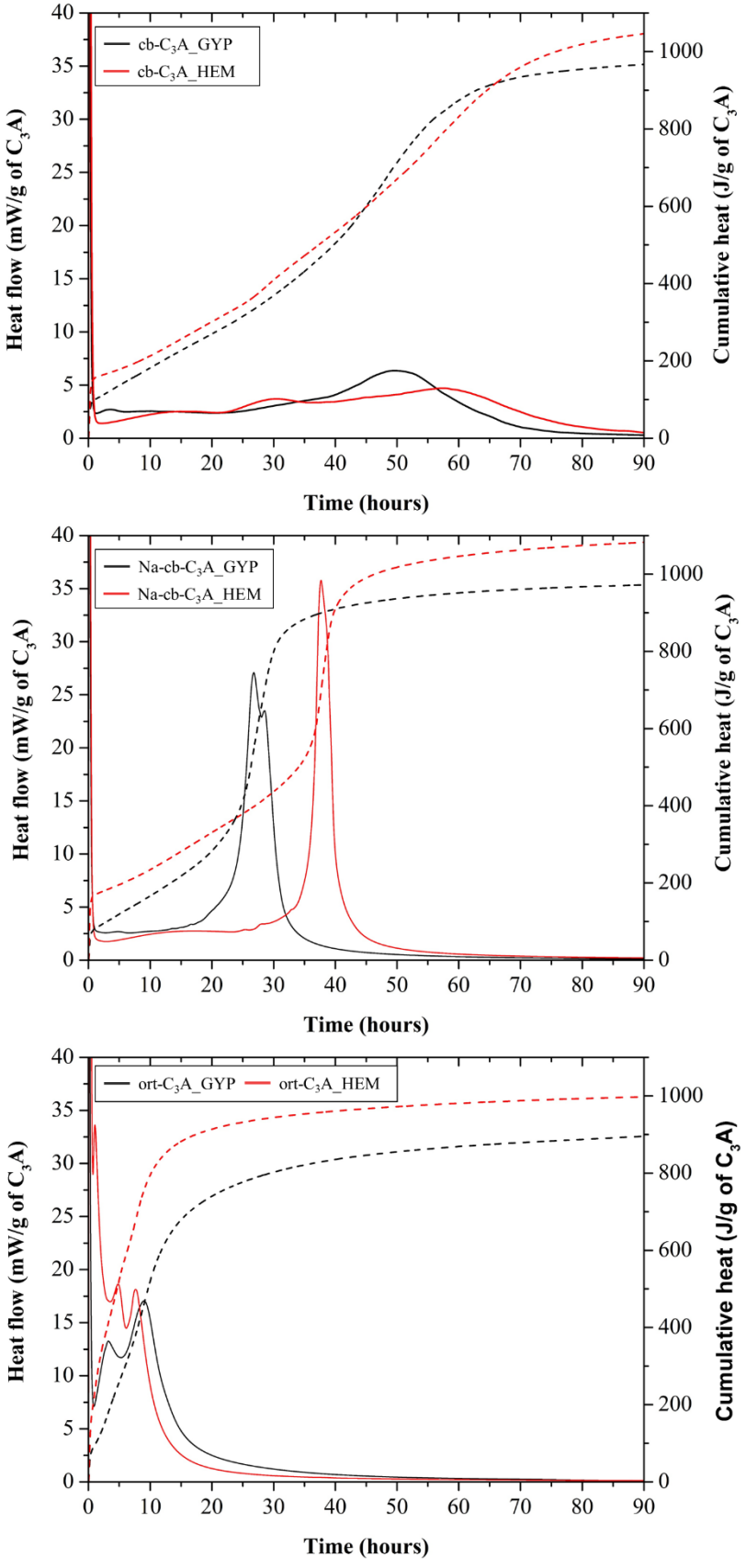

Figure 6 – Heat flow curves (solid lines and primary/left "y" axis) and cumulative heat curves (dashed lines and secondary/right "y" axis) of the (A) cb-C_3A, (B) Na-cb-C_3A, and (C) ort-C_3A pastes with gypsum and hemihydrate during the first 90 hours of hydration.

3.2 In-situ X-ray diffraction (XRD)

The set of XRD patterns of the pastes over time up to 48 hours is presented in Figure S4. Figure 7 presents some key XRD patterns. Figure 8 shows the relative scale factor of the crystalline phases over time. No bassanite (crystalline hemihydrate) was found in the pastes with hemihydrate addition (Figure 7c-d and Figure 8d-f), indicating that it converted into gypsum before the first XRD measurement (i.e., within the first 40 minutes of hydration). This is in line with that reported by Jakob et al. [4] and García-Maté et al. [63], which observed this phenomenon before 10-20 minutes of hydration.

For the cb-C_3A_GYP and Na-cb-C_3A_GYP samples (Figure 7a and b, respectively), the diffuse scattering promoted by the free water prevented the clear identification of the crystalline phases up to about 8 hours of hydration, as seen in the first two patterns of Figure 7a and Figures S4 (a,b). This issue was also reported by Scherb et al. [48] for pastes with high w/s ratios. In general, the beginning of AFm formation was identified simultaneously with the beginning of ettringite consumption as expected. The Na-cb-C_3A and ort-cb-C_3A mixes with both gypsum and hemihydrate incorporation formed U-phase as AFm, resulting from the presence of sodium either from the C_3A composition (for ort-C_3A) or from external addition (for Na-cb-C_3A), exemplified in Figures 7 (b,c,d). The presence of U-phase in these pastes agrees with previous studies [27,30,31], which observed U-phase in C_3A-gypsum pastes hydrating at 0.25-1.0 M of NaOH (note that Na-cb-C_3A is hydrating at a 0.99 M of NaOH solution).

The U-phase ($4CaO \cdot 0.9Al_2O_3 \cdot 1.1SO_3 \cdot 0.5Na_2O \cdot 16H_2O$) belongs to the group of hexagonal or pseudo-hexagonal layered structures (AFm), being similar to monosulfate but with Na between the layers and has a higher interlayer distance [28,29,64]. The U-phase is formed in the presence of SO_4^{2-} and Na^+ ions and a high alkaline medium [64]. The actual pH range that leads to U-phase formation is still not clear.

The U-phase formation occurred similarly to that usually observed for monosulfate, i. e., after the sulfate depletion, leading to a consumption of ettringite [11,33]. This ettringite consumption is expected from equilibrium conditions at the sulfate depletion since the U-phase also contains SO_4^{2-} content in its composition, but a lower content compared with ettringite.

In contrast, no AFm formation was identified in the cb-C_3A_GYP and cb-C_3A_HEM samples for up to 48 hours (see Figure 7a and Figure S4a,d). Although the gypsum depletion was identified at about 32-36 hours for these mixes (Figures 8a and 8d), the maximum ettringite content (and subsequent conversion into AFm) generally occurred a few hours after the sulfate depletion for the other mixes (Figure 8b,c,e,f). This is in line with the results reported by Jansen et al. [8], who showed that ettringite formation depends on the coupled availability of sulfur and aluminum (the latter, from C_3A dissolution). In fact, a relatively low reduction in the scale factor of C_3A was observed within the first two days of hydration in the cb-C_3A mixes with both gypsum and hemihydrate, suggesting the low consumption of C_3A and justifying the lack of AFm formation during this period. The continuous ettringite formation after gypsum depletion happened even after the gypsum depletion (observed by XRD), suggesting the presence of sulfate ions in the solution as observed by Jansen et al. [65].

Regarding the rate of hydration, the XRD results are in agreement with the calorimetry results. For the samples with gypsum, the ort-C_3A presented the earlier gypsum depletion occurring at 7.8 hours and the maximum of ettringite and beginning of U-phase formation at 11.2 hours. The Na-cb-C_3A_GYP presented gypsum depletion at 15 hours and U-phase formation at 35 hours. The cb-C_3A_GYP presented the later gypsum depletion at ~36 hours, and no AFm formation was detectable up to 48 hours.

As for the replacement of gypsum with hemihydrate, the XRD results also corroborate with the calorimetry data. This replacement led to a later start of sulfate depletion, and gypsum was still present in the cb-C_3A_HEM paste after 48 hours of hydration. The use of hemihydrate in the Na-cb-C_3A_HEM sample delayed the gypsum depletion by 17 hours and the U-phase formation by 8.9 hours compared to the Na-cb-C_3A-GYP sample. Finally, the use of hemihydrate instead of gypsum in the ort-C_3A paste led to a higher ettringite formation rate and anticipated gypsum depletion by 0.4 hours and U-phase formation by 2.2 hours.

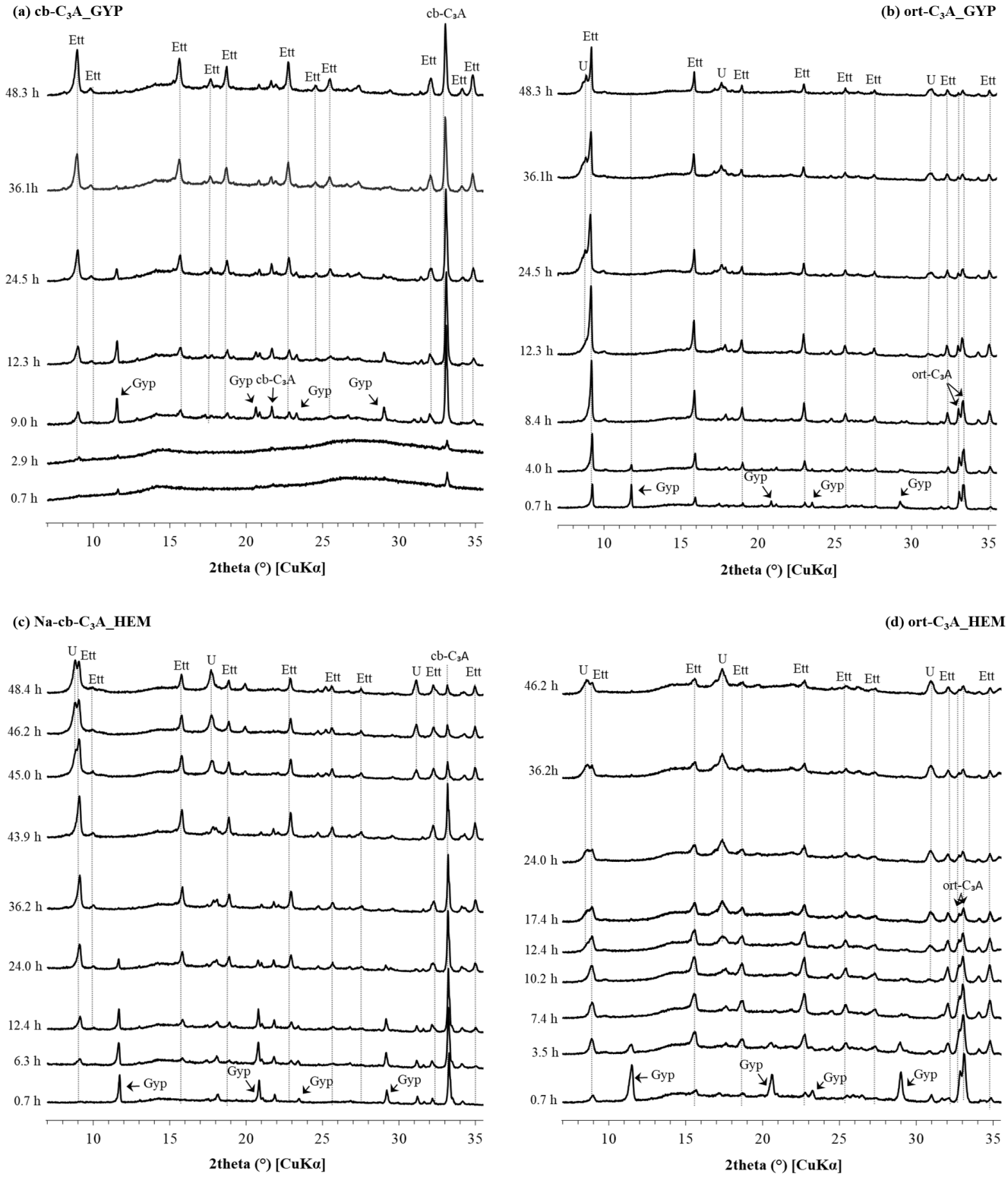

1 Figure 7 – Key XRD patterns of in-situ measurement for the different C_3A pastes with gypsum and
2 hemihydrate. Ett: ettringite, U: U-phase, Gyp: Gypsum, cb-C_3A: cubic C_3A, ort-C_3A: orthorhombic C_3A.

3

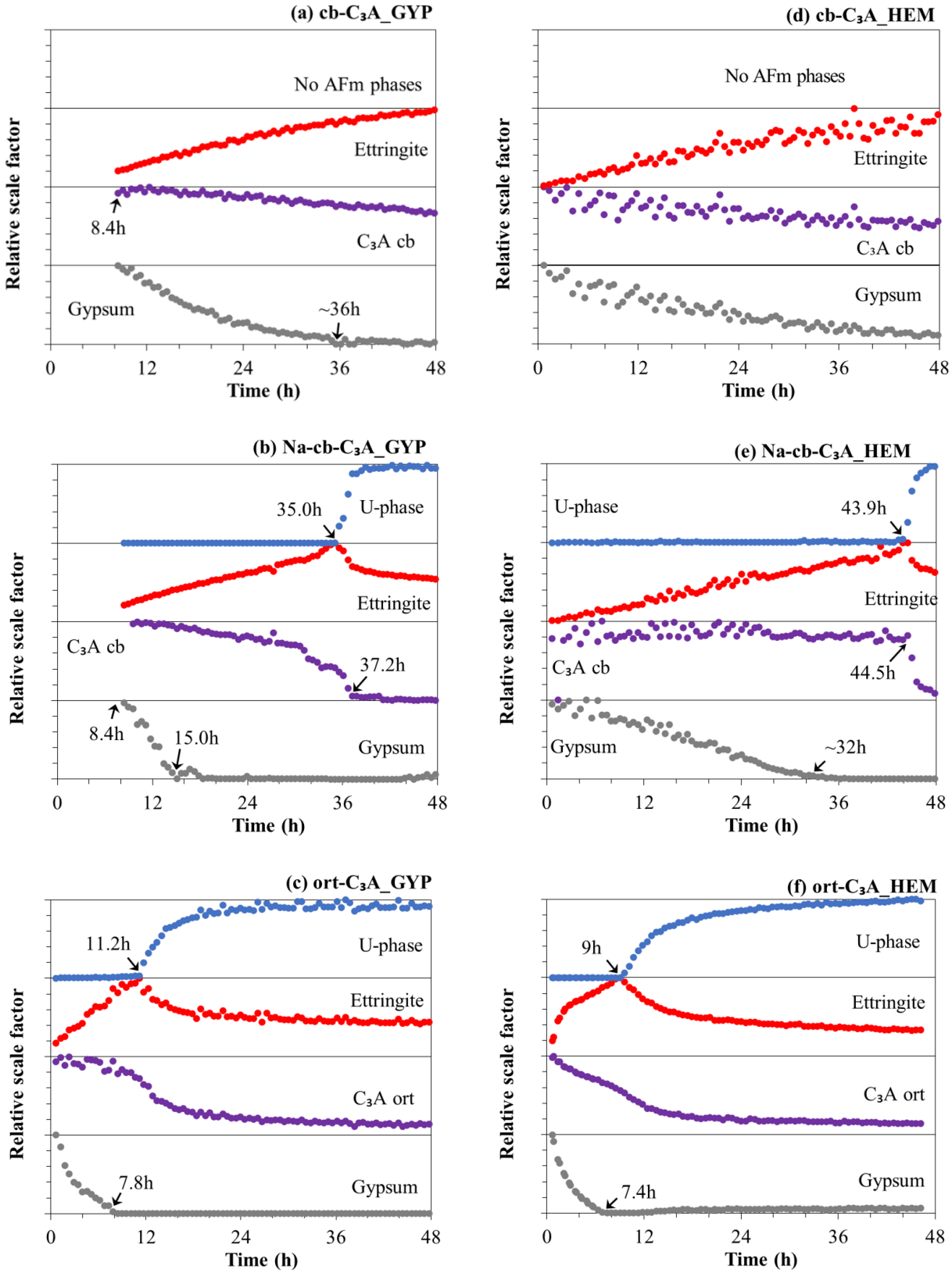

Figure 8 – Relative scale factor evolution of the crystalline phases monitored by in-situ XRD: (A) cb-C_3A-GYP, (B) Na-cb-C_3A_GYP, (C) ort-C_3A_GYP pastes, (D) cb-C_3A-HEM, (E) Na-cb-C_3A_HEM, and (F) ort-C_3A_HEM pastes during the first 48 hours of hydration. The lack of data for (a) and (b) within the first hours is explained in the text.

3.3 Thermogravimetric analysis (TGA)

Figure 9 presents the DTG curves of C_3A pastes with gypsum and hemihydrate at 1 h, 1, 2, and 3 d of hydration. Peaks related to the decomposition of ettringite (80–105 °C), gypsum (120-160 °C), AFm phases (160–190 °C and 270–300 °C), and carbonates (600–750°C) are observed [66]. Figure 10 shows the bound water content (in g/100g of paste) up to 3 days of hydration.

At 1 hour, a peak between 240-260 °C was observed for all samples but was not present at 1, 2, and 3 days. This peak corresponds to the thermal decomposition of $Al(OH)_3$ and was also observed by Myers *et al*. [17] in cb-C_3A, and ort-C_3A pastes with gypsum at 8 minutes of hydration. This phase was not detectable by XRD, which agrees with previous studies [17] that reported that this phase is poorly crystalline.

Following the trends observed in calorimetry and *in-situ* XRD, the ort-C_3A pastes reacted much faster than the cb-C_3A, and Na-cb-C_3A pastes. At 1 hour, the ort-C_3A pastes presented a higher ettringite peak, a lower gypsum peak, and a higher bound water content than the cb-C_3A pastes, indicating its higher reactivity. Furthermore, at 1 day, it is already possible to identify AFm peaks in ort-C_3A. The ort-C_3A reaction is almost complete at this age since no significant changes were observed in TGA curves from 1 to 2 and 3 days, following the calorimetry and XRD results.

NaOH also accelerated the C_3A hydration, but only after 1 day (see Figure 10). At 48 hours, the peak of gypsum dehydration is no longer present in the Na-cb-C_3A pastes, and AFm peaks appeared, which agrees with the calorimetry and XRD results. In cb-C_3A pastes, the gypsum peak is still present at 48 hours, which is also consistent with XRD results (see Figure 8). In the cb-C_3A_GYP sample, small AFm decomposition peaks are observed at 48 hours, although no AFm was observed in XRD. This discrepancy might result from the low amount of AFm phase at 48 hours in the cb-C_3A samples and of the difficulty in identifying the AFm phases in XRD due to their layered and poorly crystalline nature [43].

Regarding the replacement of gypsum with hemihydrate, the TGA results corroborate with the calorimetry and XRD results. The initial hydration of cb-C_3A and Na-cb-C_3A with gypsum and hemihydrate was very similar. However, after the first day, hemihydrate retarded the cb-C_3A and Na-cb-C_3A hydration compared to gypsum (see Figure 10). In

turn, the replacement of gypsum with hemihydrate accelerated the ort-C_3A hydration within the first day and was similar afterward.

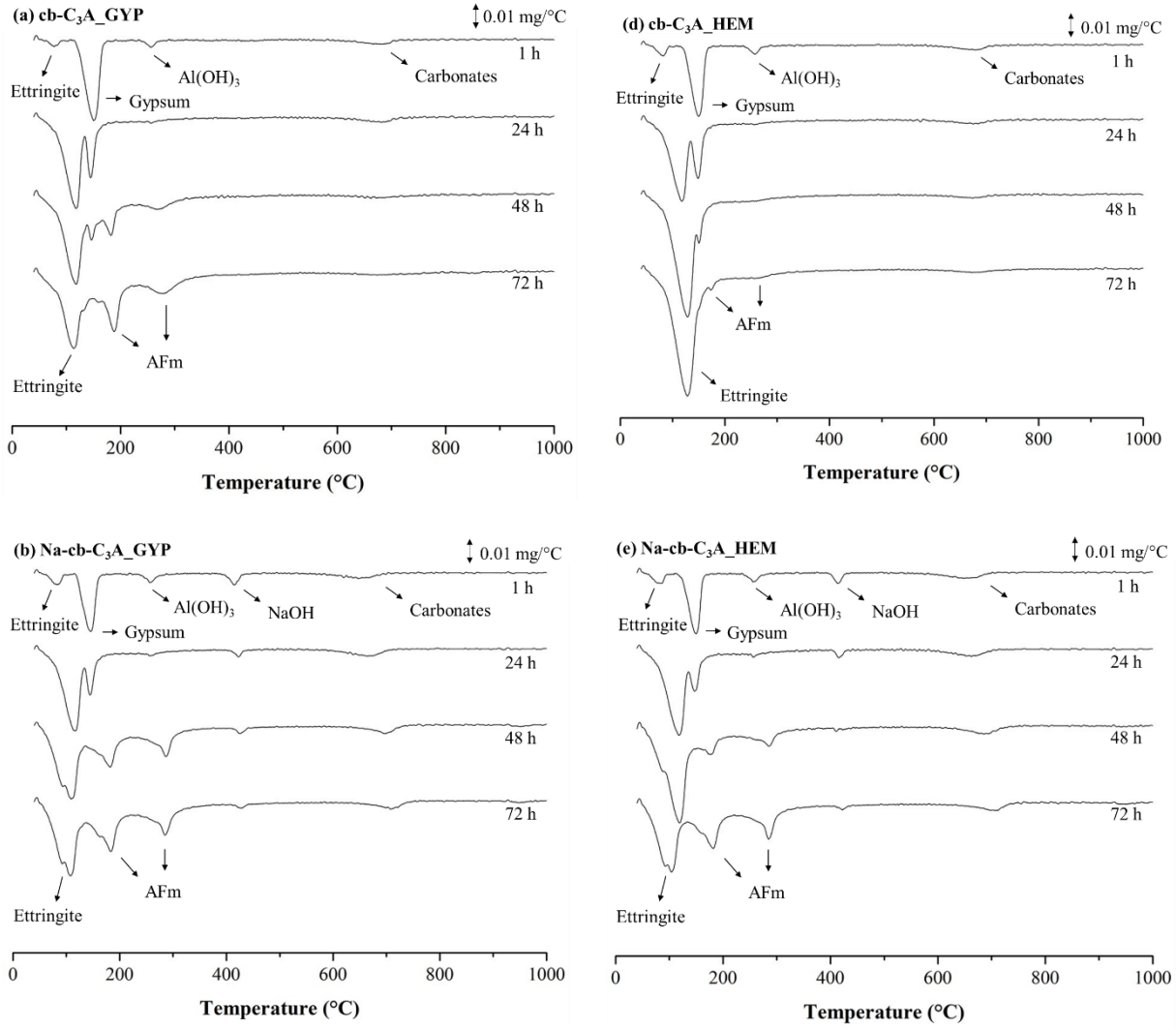

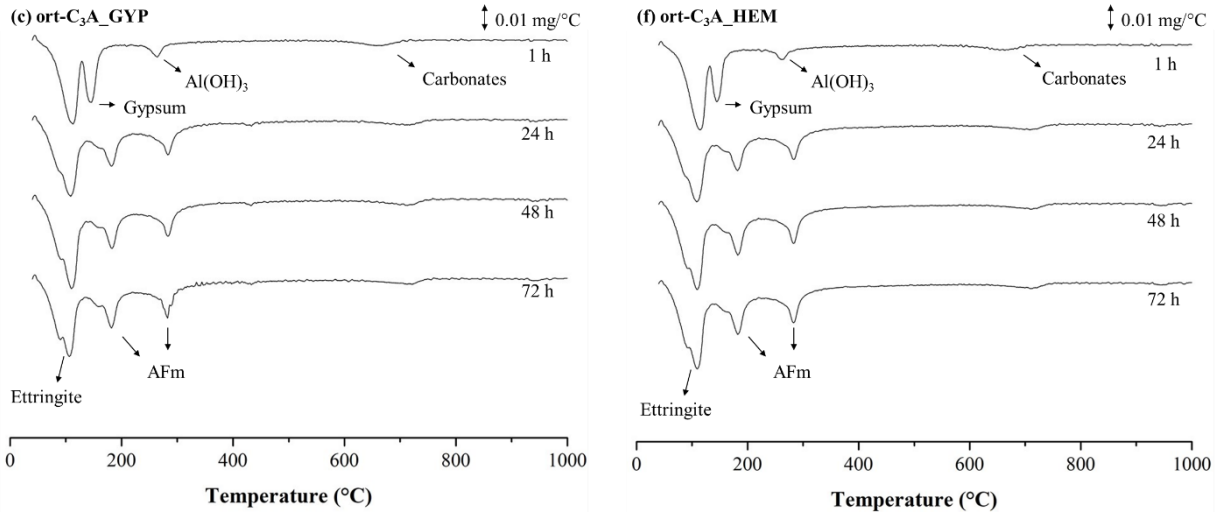

Figure 9 – DTG curves of: (A) cb-C_3A-GYP, (B) Na-cb-C_3A_GYP, (C) ort-C_3A_GYP pastes, (D) cb-C_3A-HEM, (E) Na-cb-C_3A_HEM, and (F) ort-C_3A_HEM pastes at 1 h, 24 h, 48 h, and 72 hours of hydration.

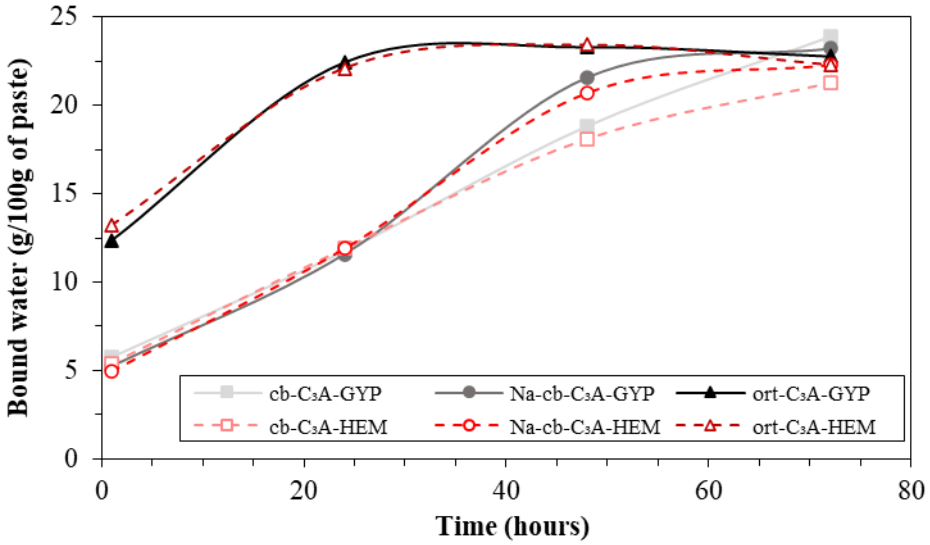

Figure 10 – Bound water content (g/100g of paste) of C_3A pastes with gypsum and hemihydrate up to 72 hours of hydration.

3.4 Rheometry

Figure 11 shows the rheological properties of the C_3A pastes produced with gypsum, and Figure 12 shows fresh pastes during the rheological tests. After 120 minutes, both mixes cb-C_3A_GYP and Na-cb-C_3A_GYP remained flowable (Figure 11a), while the ort-C_3A_GYP sample was flowable only until 70 minutes. After that, the shearing cycles could not be performed since the sample was already stiff (Figure 11b). In turn, the hemihydrate-containing samples lost their workability within the first 10 minutes of

hydration when the first shearing cycle was applied (Figure 11c); therefore, the rheological evaluation of these mixes was not able to be performed. This is due to the hydration of hemihydrate and consequent precipitation of gypsum -also observed in XRD results and SEM images (Figure S8)-, resulting in the so-called "false set" [33,67].

For all the gypsum-containing mix, the yield stress and viscosity increased exponentially over time (correlations with R^2 of 0.92-0.98). This is consistent with that reported by Jakob et al. [68], which attributed this phenomenon mainly to the change in the solid fraction with water consumption and ettringite formation over time. In addition, the needle-like shape of ettringite can increase the interparticle friction and hinder the flow, increasing the yield stress and the viscosity [69,70].

For the cubic C_3A pastes, this increase was relatively low up to 70 minutes due to the lower ettringite formation within this period, as seen in the SEM images of Figure S5(a,b) and Figure S6(a,b). At 30 minutes of hydration, only a few ettringite crystals with tenths of a micrometer were found. In turn, at 120 minutes of hydration, more ettringite crystals were found (Figure S5(c,d) and Figure S6(c,d)), corroborating with the hypothesis of Jakob et al. [68]. The presence of NaOH further increased the yield stress and viscosity of paste from 70 to 120 minutes, which can be explained by the higher reaction rate in the presence of such hydroxide (discussed in Sections 3.1–3.3).

As for the ort-C_3A_GYP paste, a significant amount of ettringite crystals can be found already at 30 minutes of hydration (Figure S7(a,b)) due to the faster ettringite formation of orthorhombic C_3A in the presence of gypsum compared with cubic C_3A, as observed by calorimetry, XRD, and TGA, and as reported by previous studies [12,17,20]. This can explain the several times greater yield stress and viscosity of the mix containing orthorhombic C_3A than those produced with cubic C_3A even at 10 minutes of hydration. These results agree with the results observed by Kirchheim et al. [10], who observed that the ort-C_3A-GYP pastes presented storage modulus (G') three times higher (*i. e.*, lower fluidity) than the cb-C_3A-GYP pastes.

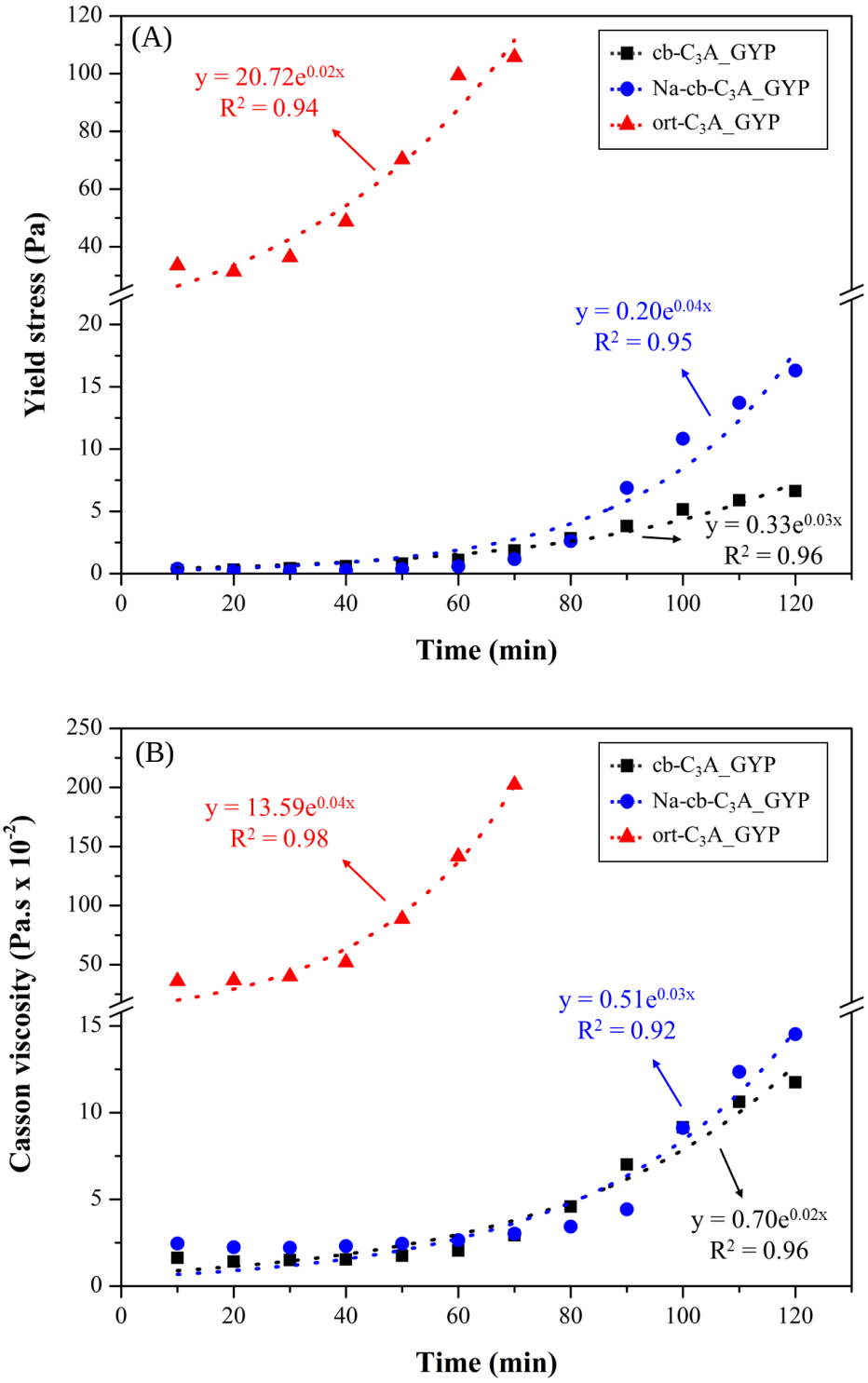

Figure 11 – (A) yield stress and (B) Casson viscosity of C_3A-gypsum pastes up to 120 min of hydration.

Figure 12 – Fresh pastes during the rheological tests. (a) cb-C_3A_GYP after 120 minutes; (b) ort-C_3A_GYP after 120 minutes; (c) cb-C_3A_HEM after 10 minutes.

4 DISCUSSION

4.1 The role of sodium on the hydration of C_3A

As observed in this study and by several authors [12,17,20], pure ort-C_3A reacts much faster than cb-C_3A in the presence of calcium sulfates. The reason for that is not apparent yet. However, two main hypotheses exist to explain this behavior: (*i*) the dissolution of ort-C_3A releases sodium into the solution, increasing its alkalinity, which would destabilize the amorphous alumina layer preventing the adsorption of SO_4^{2-} and/or Ca–S ion-pair [16]; and (*ii*) sodium-doping increases the solubility of the ring structures of $Al_6O_{18}^{18-}$, which would impair the formation of the Al-rich leached layer on the C_3A particles, inhibiting the adsorption of SO_4^{2-} and/or Ca–S ion-pair [12,17]. The first hypothesis relates this behavior to the presence of sodium in the solution, while the second relates it to the differences in the crystal structure.

As revealed by our calorimetry, *in-situ* XRD, and TGA, the external sodium incorporation (i.e., the addition of NaOH) did not significantly affect cb-C_3A hydration in the first hours (up to 20-24 hours) but enhanced it after that. In turn, the Na-doped C_3A crystals (i.e., ort-C_3A) had a much higher hydration rate from the beginning, with almost all the C_3A reacted within the first day. From our results, hypothesis (*i*) looks unlikely since, in the Na-cb-C_3A systems, all the sodium was already dissolved in the solution, while the sodium of ort-C_3A was gradually released with its dissolution. Therefore, hypothesis (*i*) predicted that Na-cb-C_3A to react faster than ort-C_3A, which was not validated experimentally. In turn, the predictions of hypothesis (*ii*) agree well with our results: the

much higher ort-C_3A reactivity in sulfate-containing solution is related to the difference in crystal structure rather than the presence of sodium in the solution.

The external addition of NaOH anticipated the onset of the second peak and increased the second peak intensity. As observed in Figure S2, the NaOH amount did not impact the moment of the onset, and all samples with NaOH presented the onset of the main hydration peak around 15 hours (*i.e.*, ≈ 10 hours earlier than the cb-C_3A-GYP paste). However, the greater is the NaOH amount (*i.e.*, the higher the NaOH molarity), the higher is the main heat flow peak.

The anticipation of the onset of the second peak due to the NaOH is probably related to the higher solubility of gypsum in NaOH highly alkaline solutions [71]. As observed by Ghorab and Abou El Fetouh [71], gypsum dissolution increases with the increase of NaOH molarity up to 0.05 M of NaOH and remains constant afterward. The higher solubility of gypsum in the NaOH solution anticipates the gypsum depletion -as observed by XRD-, and therefore anticipates the onset of the main heat flow peak -as observed by calorimetry. In addition, as all solutions evaluated here had NaOH molarities higher than 0.05 M (0.24, 0.48, and 0.99 M), gypsum solubility should be similar among these solutions according to the Ghorab and Abou El Fetouh [71] results, which explains why the NaOH molarity did not impact the moment of the onset of the main heat flow peak.

In turn, the increase of the main heat flow peak intensity with the increase of NaOH molarity indicates an increase in the AFm precipitation rate [11]. This is probably related to the amount of Na^+ available for the formation of the U-phase (the only AFm observed in the Na-containing samples). This would increase the rate of U-phase formation, as observed by the higher heat flow peak in Figure S2, but probably did not alter the amount of U-phase formed by the end of the 90 hours, as the cumulative heat was similar. The amount of U-phase formed is depended on the relation between gypsum and C_3A, and as was the same for all the samples, it did not change. Further studies on this topic are encouraged to additional conclusions.

In both Na-cb-C_3A and ort-C_3A pastes, U-phase was formed instead of monosulfate after sulfate depletion. This occurred because sodium was incorporated into the interlayer space of AFm. The U-phase formation led to a decrease in the ettringite content, similar to what is observed during the formation of monosulfate, and this was expected since the

U-phase ($4CaO \cdot 0.9Al_2O_3 \cdot 1.1SO_3 \cdot 0.5Na_2O \cdot 16H_2O$) contains sulfate in its composition. Since there is no more sulfate available in the solution, a portion of ettringite decomposed, releasing the sulfate ions required for U-phase formation.

4.2 The effect of hemihydrate on the hydration of C_3A polymorphs

The replacement of gypsum with hemihydrate did not have a great impact on the cb-C_3A but delayed the sulfate depletion and the AFm phase formation of the Na-cb-C_3A paste. In turn, for the ort-C_3A, the use of hemihydrate resulted in faster ettringite precipitation and earlier sulfate depletion and U-phase formation when compared to the pastes with gypsum, as shown by calorimetry, XRD, and TGA.

Porchet et al. [35] observed an acceleration in cb-C_3A hydration when replaced gypsum with hemihydrate (when using less than 15 wt% equivalents of gypsum by wt% of C_3A amount). In turn, they observed a delay in cb-C_3A hydration when using higher amounts of calcium sulfate (more than 15 wt% equivalents of gypsum by wt% of C_3A). The reasons for that are still not clear.

Pourchet *et al*. [35] have observed that the use of hemihydrate instead of gypsum in cb-C_3A pastes increases the concentration of Ca and SO_4 in the pore solution, leading to higher super saturation degrees with regarding to the ettringite. As pointed out by the authors, according to the classical nucleation theory, the frequency of nucleation increases with the increase of the supersaturation degree. Therefore, the higher solubility of hemihydrate may contribute to the increase of ettringite nucleation, with a greater quantity of nuclei, accelerating the ettringite formation and, thus, the sulfate consumption. However, the reason for this only accelerated the sulfate depletion on ort-C_3A and not on cb-C_3A (at least at the gypsum/C_3A ratio used here) is not clear yet. Thus, further studies on this topic are necessary to fully understand the influence of the sulfate source solubility on cb-C_3A and ort-C_3A hydration.

Finally, for all pastes, the use of hemihydrate resulted in early stiffing (the so-called false setting) due to the formation of larger gypsum crystals in the first minutes, as observed by XRD and SEM and also reported in previous studies. This might have important implications for fresh PC concrete, as discussed in the next section.

4.3 Implications for fresh PC concrete

The much higher reactivity of ort-C_3A in sulfate-containing solution, compared with cb-C_3A may lead to setting and/or rheology problems in fresh PC concrete. Furthermore, the higher rate of ettringite formation and sulfate depletion may result in sulfate balance issues, leading to undersulfated mixtures, negatively impacting the rheology and early strength of PC concrete.

However, note that there are essential differences between the pure phases -as those studied here- and the phases present in commercial PC, such as the type of alkalis incorporated (in commercial cements, K_2O is usually incorporated in the C_3A structure, while Na_2O is generally used for the synthesis of orthorhombic C_3A in the laboratory); the incorporation of other ions (such as Fe); different particle size distribution and surface area; and mainly the interactions with other clinker phases needs to be kept in mind. Thus, although it is easier to isolate the actuation mechanisms in pure phase systems, further studies with industrial clinkers with different C_3A polymorphs evaluating the sulfate balance, rheology, hydration, and strength are necessary to understand the impact of ort-C_3A on PC concrete fully.

Finally, the use of hemihydrate as the sulfate source may lead to early stiffing (i.e., false set) due to its crystallization into gypsum, as observed in previous studies [67,72] and in the current work, which impairs concrete application and performance. Therefore, the cement industry must control the grinding process to avoid the transformation of gypsum into hemihydrate. Furthermore, since hemihydrate intensifies ort-C_3A reaction, it can also intensify the application issues of ort-C_3A previously discussed.

5 CONCLUSIONS

This study has spread light to:

- The orthorhombic C_3A presented faster ettringite precipitation in the first hours and a much earlier sulfate depletion and AFm precipitation compared with cubic C_3A. This is probably related to the differences in crystal structure rather than the release of sodium and the increase of solution alkalinity. The external addition of sodium (i.e., NaOH incorporation) in cubic C_3A paste anticipated the sulfate

depletion and the new fast C_3A dissolution. However, it did not significantly influence the cubic C_3A hydration in the first 20-24 hours, while the orthorhombic C_3A had almost entirely reacted by then.

- In pastes with cubic C_3A + NaOH or orthorhombic C_3A, U-phase was formed instead of monosulfate after sulfate depletion, leading to a decrease in ettringite content.

- Orthorhombic C_3A paste produced with gypsum presented viscosity and yield stress values 10-20 times higher than those containing cubic C_3A with and without NaOH, as a result of its much higher reactivity and quick formation of larger ettringite crystals in the first minutes.

- The replacement of gypsum with hemihydrate (in an SO_3/C_3A ratio of 0.29) did not significantly influence cb-C_3A hydration. However, the use of hemihydrate instead of gypsum retarded Na-cb C_3A hydration, delaying the sulfate depletion and AFm formation. In contrast, it had an opposite effect on the hydration of orthorhombic C_3A, increasing the ettringite formation rate and anticipating the sulfate depletion and AFm formation.

- The use of hemihydrate in pastes with either cubic or orthorhombic C_3A resulted in early stiffing (the so-called false set) within the first 10 minutes due to the hydration of hemihydrate and precipitation of larger gypsum crystals, making it lose workability.

Future studies comparing the pore solution composition and pH of the orthorhombic C_3A and cubic C_3A hydrating at NaOH solutions are encouraged to fully understand the main mechanism responsible for the higher ettringite precipitation and early sulfate depletion of orthorhombic C_3A. In addition, future studies with industrial clinkers should address the implications of the difference of C_3A polymorphism on the PC properties (sulfate balance, rheology, hydration, and strength). The impact of the solubility of the calcium sulfate on cubic and orthorhombic C_3A needs more studies to clarify its mechanisms. Finally, more studies regarding the U-phase are necessary.

6 ACKNOWLEDGEMENTS

JSAN, PEM, and PJPG thanks the financial support of CAPES (Coordination for the Improvement of Higher Education Personnel) [88882.439908/2019-01]. JSAN thanks the University of Malaga (Spain), where the experiments for the characterization of the raw materials were performed. JSAN and AGdT also thank the Spanish Junta de Andalucía [P18-RT-720] research project for the research stage at the University of Málaga (Spain) and the Graduate Program in Civil Engineering: Construction and Infrastructure (PPGCI) of the Federal University of Rio Grande do Sul (UFRGS). PRM and PJPG thank the Brazilian funding agency FAPESC. The participation APK and CEMC were sponsored by CNPq (Brazilian National Council for Scientific and Technological Development) through the research fellowships PQ2017 305530/2017- 8 and PQ2019 304756/2019-9. The in-situ XRD data collection was carried out by PRM and CEMC at Laboratório de Difração de Raios-X (LDRX-UFSC). Ms. Patrícia Prates from Laboratório de Materiais (LabMAT-UFSC) is kindly acknowledged for the assistance in the SEM analysis.

7 REFERENCES

[1] F. Nishi, Y. Takeuchi, The A16018 Rings of Tetrahedra in the Structure of Cas.sNaA16O18, Acta Crystallographica Section B Structural Crystallography and Crystal Chemistry. 31 (1975) 1169–1173.

[2] Y. Takeuchi, F. Nishi, I. Maki, Structural aspects of the C3A-Na20 solid solutions, in: Proc. 7th International Congress on the Chemistry of Cement, Paris, 1980.

[3] H.F.W. Taylor, Cement chemistry, 2nd ed., Thomas Telford, 1997. https://doi.org/10.1680/cc.25929.

[4] Y. Takéuchi, F. Nishi, Crystal-chemical characterization of the 3 CaO.Al2O3 solid-solution series, Zeitschrift Für Kristallographie. 152 (1980) 259–307.

[5] K. Fukuda, S. Inoue, H. Yoshida, Cationic substitution in tricalcium aluminate, Cement and Concrete Research. 33 (2003) 1771–1775. https://doi.org/10.1016/S0008-8846(03)00172-8.

[6] A.I. Boikova, A.I. Domansky, V.A. Paramonova, THE INFLUENCE OF Na20 ON THE STRUCTURE AND PROPERTIES OF 3CaO.Al203, 7 (1977) 483–491.

[7] P. Mondal, J.W. Jeffery, The Crystal Structure of Triealeium Aluminate, Ca3Al2O6, Acta Crystallographica. (1975) 689.

[8] A.P. Kirchheim, D.C. Dal Molin, P. Fischer, A.H. Emwas, J.L. Provis, P.J.M. Monteiro, Real-time high-resolution X-ray imaging and nuclear magnetic resonance study of the hydration of pure and Na-doped C3A in the presence of sulfates, Inorganic Chemistry. 50 (2011) 1203–1212. https://doi.org/10.1021/ic101460z.

[9] K.L. Scrivener, A. Nonat, Hydration of cementitious materials, present and future, Cement and Concrete Research. 41 (2011) 651–665. https://doi.org/10.1016/j.cemconres.2011.03.026.

[10] A.P. Kirchheim, V. Fernàndez-Altable, P.J.M. Monteiro, D.C.C. Dal Molin, I. Casanova, Analysis of cubic and orthorhombic C3A hydration in presence of gypsum and lime, Journal of Materials Science. 44 (2009) 2038–2045. https://doi.org/10.1007/s10853-009-3292-3.

[11] A. Quennoz, K.L. Scrivener, Hydration of C 3A-gypsum systems, Cement and Concrete Research. 42 (2012) 1032–1041. https://doi.org/10.1016/j.cemconres.2012.04.005.

[12] A.P. Kirchheim, E.D. Rodríguez, R.J. Myers, L.A. Gobbo, P.J.M. Monteiro, D.C.C. Dal Molin, R.B. de Souza, M.A. Cincotto, Effect of gypsum on the early hydration of cubic and Na-doped orthorhombic tricalcium aluminate, Materials. 11 (2018) 1–16. https://doi.org/10.3390/ma11040568.

[13] S. Joseph, J. Skibsted, Ö. Cizer, A quantitative study of the C3A hydration, Cement and Concrete Research. 115 (2019) 145–159. https://doi.org/10.1016/j.cemconres.2018.10.017.

[14] T. Matschei, B. Lothenbach, F.P. Glasser, The role of calcium carbonate in cement hydration, Cement and Concrete Research. 37 (2007) 551–558. https://doi.org/10.1016/j.cemconres.2006.10.013.

[15] T. Matschei, B. Lothenbach, F.P. Glasser, The AFm phase in Portland cement, Cement and Concrete Research. 37 (2007) 118–130. https://doi.org/10.1016/j.cemconres.2006.10.010.

[16] D. Stephan, S. Wistuba, Crystal structure refinement and hydration behaviour of doped tricalcium aluminate, Cement and Concrete Research. 36 (2006) 2011–2020. https://doi.org/10.1016/j.cemconres.2006.06.001.

[17] R.J. Myers, G. Geng, E.D. Rodriguez, P. da Rosa, A.P. Kirchheim, P.J.M. Monteiro, Solution chemistry of cubic and orthorhombic tricalcium aluminate hydration, Cement and Concrete Research. 100 (2017) 176–185. https://doi.org/10.1016/j.cemconres.2017.06.008.

[18] A.P. Kirchheim, D.C. Dal Molin, P. Fischer, A.H. Emwas, J.L. Provis, P.J.M. Monteiro, Real-time high-resolution X-ray imaging and nuclear magnetic resonance study of the hydration of pure and Na-doped C3A in the presence of sulfates, Inorganic Chemistry. 50 (2011) 1203–1212. https://doi.org/10.1021/ic101460z.

[19] J. Cheung, A. Jeknavorian, L. Roberts, D. Silva, Impact of admixtures on the hydration kinetics of Portland cement, Cement and Concrete Research. 41 (2011) 1289–1309. https://doi.org/10.1016/j.cemconres.2011.03.005.

[20] M.M. Alonso, F. Puertas, Adsorption of PCE and PNS superplasticisers on cubic and orthorhombic C3A. Effect of sulfate, Construction and Building Materials. 78 (2015) 324–332. https://doi.org/10.1016/j.conbuildmat.2014.12.050.

[21] E. Dubina, J. Plank, L. Black, L. Wadsö, Impact of environmental moisture on C3A polymorphs in the absence and presencemof CaSO4 .0.5H2O, Advance and Cement Research. 26 (2014) 29–40.

[22] E. Dubina, J. Plank, L. Black, Impact of water vapour and carbon dioxide on surface composition of C3A polymorphs studied by X-ray photoelectron spectroscopy, Cement and Concrete Research. 73 (2015) 36–41. https://doi.org/10.1016/j.cemconres.2015.02.026.

[23] R.J. Myers, G. Geng, J. Li, E.D. Rodríguez, J. Ha, P. Kidkhunthod, G. Sposito, L.N. Lammers, A.P. Kirchheim, P.J.M. Monteiro, Role of adsorption phenomena in cubic tricalcium aluminate dissolution, Langmuir. 33 (2016) 45–55. https://doi.org/10.1021/acs.langmuir.6b03474.

[24] G. Geng, R.J. Myers, Y.-S. Yu, D.A. Shapiro, R. Winarski, P.E. Levitz, D.A.L. Kilcoyne, P.J.M. Monteiro, Synchrotron X-ray nanotomographic and spectromicroscopic study of the tricalcium aluminate hydration in the presence of gypsum, Cement and Concrete Research. 111 (2018) 130–137. https://doi.org/10.1016/j.cemconres.2018.06.002.

[25] X. Liu, P. Feng, C. Lyu, S. Ye, The role of sulfate ions in tricalcium aluminate hydration: New insights, Cement and Concrete Research. 130 (2020) 105973. https://doi.org/10.1016/j.cemconres.2020.105973.

[26] F.P. Glasser, M.B. Marinho, Early stages of the hydration of tricalcium aluminate and its sodium-cotaining solid solutions, Proceedings of the British Ceramic Society. 35 (1984) 221–236.

[27] Y. Shimada, J.F. Young, Thermal stability of ettringite in alkaline solutions at 80 j C, 34 (2004) 2261–2268. https://doi.org/10.1016/j.cemconres.2004.04.008.

[28] G. Li, P. le Bescop, M. Moranville, The U phase formation in cement-based systems containing high amounts of Na2SO4, Cement and Concrete Research. 26 (1996) 27–33. https://doi.org/https://doi.org/10.1016/0008-8846(95)00189-1.

[29] G. Li, P. le Bescop, M. Moranville-Regourd, Synthesis of the U phase (4CaO . 0.9Al2O3 . 1.1SO3. 0.5Na2O . 16H2O), Cement and Concrete Research. 27 (1997) 7–13. https://doi.org/10.1016/S0008-8846(96)00194-9.

[30] B.A. Clark, P.W. Brown, Formation of ettringite from monosubstituted calcium sulfoaluminate hydrate and gypsum, Journal of the American Ceramic Society. 82 (1999) 2900–2905. https://doi.org/10.1111/j.1151-2916.1999.tb02174.x.

[31] B.A. Clark, P.W. Brown, Formation of calcium sulfoaluminate hydrate compounds. Part II, Cement and Concrete Research. 30 (2000) 233–240. https://doi.org/10.1016/S0008-8846(99)00234-3.

[32] S.J. Way, A. Shayan, Early hydration of a portland cement in water and sodium hydroxide solutions: Composition of solutions and nature of solid phases, Cement and Concrete Research. 19 (1989) 759–769. https://doi.org/10.1016/0008-8846(89)90046-X.

[33] J. da S. Andrade Neto, A.G. de la Torre, A.P. Kirchheim, Effects of sulfates on the hydration of Portland cement – A review, Construction and Building Materials. 279 (2021). https://doi.org/10.1016/j.conbuildmat.2021.122428.

[34] V.H. Dodson, T.D. Hayden, Another look at the Portland cement/chemical admixture incompatibility problem, Cement, Concrete and Aggregates. 11 (1989) 52–56. https://doi.org/10.1520/cca10102j.

[35] S. Pourchet, L. Regnaud, J.P. Perez, A. Nonat, Early C3A hydration in the presence of different kinds of calcium sulfate, Cement and Concrete Research. 39 (2009) 989–996. https://doi.org/10.1016/j.cemconres.2009.07.019.

[36] F. Zunino, K. Scrivener, Factors influencing the sulfate balance in pure phase C3S/C3A systems, Cement and Concrete Research. 133 (2020) 106085. https://doi.org/10.1016/j.cemconres.2020.106085.

[37] P.J. Sandberg, L.R. Roberts, Cement-Admixture Interactions Related to Aluminate Control, 2 (2005) 1–14.

[38] P.K. Mehta, P.J.M. Monteiro, Concrete: Microstructure, Properties, and Materials, 4th ed., McGraw-Hill Professional Publishing, 2014.

[39] P.J. Sandberg, L.R. Roberts, Cement-admixture interactions related to aluminate control, Journal of ASTM International. 2 (2005) 219–232. https://doi.org/10.1520/jai12296.

[40] M. Palacios, H. Kazemi-Kamyab, S. Mantellato, P. Bowen, Laser diffraction and gas adsorption techniques, in: K. Scrivener, R. Snellings, B. Lothenbach (Eds.), A Practical Guide to Microstructural Analysis of Cementitious Materials, 1st ed., CRC Press, 2016: pp. 445–480.

[41] L. Black, C. Breen, J. Yarwood, C.-S. Deng, J. Phipps, G. Maitland, Hydration of tricalcium aluminate (C A) in the presence and absence of gypsum—studied by Raman spectroscopy and X-ray diffraction, Journal of Materials Chemistry. (2006) 1–21. https://doi.org/https://doi.org/10.1039/B509904H.

[42] L. Wadsö, Operational issues in isothermal calorimetry, Cement and Concrete Research. 40 (2010) 1129–1137. https://doi.org/10.1016/j.cemconres.2010.03.017.

[43] D. Ectors, Advances in the analysis of cementitious reactions and hydrate phases, 2016.

[44] F. Goetz-Neunhoeffer, J. Neubauer, Refined ettringite (Ca 6 Al 2 (SO 4) 3 (OH) 12 ·26H 2 O) structure for quantitative X-ray diffraction analysis , Powder Diffraction. 21 (2006) 4–11. https://doi.org/10.1154/1.2146207.

[45] Á.G. de la Torre, M.-G. López-Olmo, C. Álvarez-Rua, S. García-Granda, Miguel.A.G. Aranda, Structure and microstructure of gypsum and its relevance to Rietveld quantitative phase analyses, Powder Diffraction. 19 (2004) 240–246. https://doi.org/10.1154/1.1725254.

[46] C. Bezou, A. Nonat, J.C. Mutin, A. Nørlund Christensen, M.S. Lehmann, Investigation of the crystal structure of γ-CaSO4, CaSO4 · 0.5 H2O, and CaSO4 · 0.6 H2O by powder diffraction

methods, Journal of Solid State Chemistry. 117 (1995) 165–176. https://doi.org/10.1006/jssc.1995.1260.

[47] K. Post, H. Pollmann, PDF 00-044-0272, ICDD Grant-in-Aid, Friedrich-Alexander-Universität. (1992).

[48] S. Scherb, N. Beuntner, K.C. Thienel, J. Neubauer, Quantitative X-ray diffraction of free, not chemically bound water with the PONKCS method, Journal of Applied Crystallography. 51 (2018) 1535–1543. https://doi.org/10.1107/S1600576718012888.

[49] C. Guo, E. Wang, X. Hou, J. Chen, W. Zhang, J. Ye, Characterization and mechanism of early hydration of calcium aluminate cement with anatase-TiO 2 nanospheres additive, Construction and Building Materials. 261 (2020) 119922. https://doi.org/10.1016/j.conbuildmat.2020.119922.

[50] L.J. Gardner, S.A. Walling, C.L. Corkhill, S.A. Bernal, V. Lejeune, M.C. Stennett, J.L. Provis, N.C. Hyatt, Cement and Concrete Research Temperature transformation of blended magnesium potassium phosphate cement binders, Cement and Concrete Research. 141 (2021) 106332. https://doi.org/10.1016/j.cemconres.2020.106332.

[51] C. Shunman, A. Wu, W. Yiming, W. Wei, Coupled effects of curing stress and curing temperature on mechanical and physical properties of cemented paste backfill, Construction and Building Materials. 273 (2021) 121746. https://doi.org/10.1016/j.conbuildmat.2020.121746.

[52] A. Quennoz, K.L. Scrivener, Interactions between alite and C3A-gypsum hydrations in model cements, Cement and Concrete Research. 44 (2013) 46–54. https://doi.org/10.1016/j.cemconres.2012.10.018.

[53] R.J. Hill, C.J. Howard, Quantitative phase analysis from neutron powder diffraction data using the Rietveld method, Journal of Applied Crystallography. 20 (1987) 467–474. https://doi.org/10.1107/S0021889887086199.

[54] P. Thompson, D.E. Cox, J.B. Hastings, Rietveld Refinement of Debye-Scherrer Synchrotron X-ray Data from Al203, Journal of Applied Crystallography. 20 (1987) 79–83.

[55] W.A. Dollase, Correction of Intensities for Preferred Orientation in Powder Diffractometry: Application of the March Model, Journal of Applied Crystallography. 19 (1986) 267–272.

[56] J.D. Zea-Garcia, A.G. de la Torre, M.A.G. Aranda, I. Santacruz, Processing and characterisation of standard and doped alite-belite-ye'elimite ecocement pastes and mortars, Cement and Concrete Research. 127 (2020). https://doi.org/10.1016/j.cemconres.2019.105911.

[57] N. Casson, A Flow Equation for Pigment-Oil Suspensions of the Printing Ink Type, in: C.C. Mill (Ed.), Rheology of Disperse Systems, Pergamon Press, Oxford, 1959: pp. 84–104.

[58] H. Li, S. Ding, L. Zhang, J. Ouyang, B. Han, Rheological behaviors of cement pastes with multi-layer graphene, Construction and Building Materials. 269 (2021) 121327. https://doi.org/10.1016/j.conbuildmat.2020.121327.

[59] X. Zhang, J. Han, The effect of ultra-fine admixture on the rheological property of cement paste, Cement and Concrete Research. 30 (2000) 827–830. https://doi.org/10.1016/S0008-8846(00)00236-2.

[60] M. Nehdi, M.A. Rahman, Estimating rheological properties of cement pastes using various rheological models for different test geometry, gap and surface friction, Cement and Concrete Research. 34 (2004) 1993–2007. https://doi.org/10.1016/j.cemconres.2004.02.020.

[61] H. Minard, S. Garrault, L. Regnaud, A. Nonat, Mechanisms and parameters controlling the tricalcium aluminate reactivity in the presence of gypsum, Cement and Concrete Research. 37 (2007) 1418–1426. https://doi.org/10.1016/j.cemconres.2007.06.001.

[62] A.S. Brand, S.B. Feldman, P.E. Stutzman, A. v. Ievlev, M. Lorenz, D.C. Pagan, S. Nair, J.M. Gorham, J.W. Bullard, Dissolution and initial hydration behavior of tricalcium aluminate in low activity sulfate solutions, Cement and Concrete Research. 130 (2020) 105989. https://doi.org/10.1016/j.cemconres.2020.105989.

[63] M. García-Maté, A.G. de La Torre, L. León-Reina, E.R. Losilla, M.A.G. Aranda, I. Santacruz, Effect of calcium sulfate source on the hydration of calcium sulfoaluminate eco-cement, Cement and Concrete Composites. 55 (2015) 53–61. https://doi.org/10.1016/j.cemconcomp.2014.08.003.

[64] M.J. Sánchez-Herrero, A. Fernández-Jiménez, A. Palomo, C4A3Š hydration in different alkaline media, Cement and Concrete Research. 46 (2013) 41–49. https://doi.org/10.1016/j.cemconres.2013.01.008.

[65] D. Jansen, Ch. Naber, D. Ectors, Z. Lu, X.-M. Kong, F. Goetz-Neunhoeffer, J. Neubauer, The early hydration of OPC investigated by in-situ XRD, heat flow calorimetry, pore water analysis and 1H NMR: Learning about adsorbed ions from a complete mass balance approach, Cement and Concrete Research. 109 (2018) 230–242. https://doi.org/10.1016/j.cemconres.2018.04.017.

[66] B. Lothenbach, P.T. Durdziński, K. de Weerdt, Thermogravimetric analysis, in: K. Scrivener, R. Snellings, B. Lothenbach (Eds.), A Practical Guide to Microstructural Analysis of Cementitious Materials, 1st ed., CRC Press, 2016: pp. 177–212.

[67] C.W. Chung, P. Suraneni, J.S. Popovics, L.J. Struble, Using ultrasonic wave reflection to monitor false set of cement paste, Cement and Concrete Composites. 84 (2017) 10–18. https://doi.org/10.1016/j.cemconcomp.2017.08.010.

[68] C. Jakob, D. Jansen, N. Ukrainczyk, E. Koenders, U. Pott, D. Stephan, J. Neubauer, Relating ettringite formation and rheological changes during the initial cement hydration: A comparative study applying XRD analysis, rheological measurements and modeling, Materials. 12 (2019). https://doi.org/10.3390/ma12182957.

[69] R. Talero, C. Pedrajas, M. González, C. Aramburo, A. Blázquez, V. Rahhal, Role of the filler on Portland cement hydration at very early ages: Rheological behaviour of their fresh cement pastes, Construction and Building Materials. 151 (2017) 939–949. https://doi.org/10.1016/j.conbuildmat.2017.06.006.

[70] P.R. de Matos, L.R. Prudêncio, R. Pilar, P.J.P. Gleize, F. Pelisser, Use of recycled water from mixer truck wash in concrete: Effect on the hydration, fresh and hardened properties, Construction and Building Materials. 230 (2020) 116981. https://doi.org/10.1016/j.conbuildmat.2019.116981.

[71] H.Y. Ghorab, S.H. Abou el Fetou, Factors Affecting the Solubility of Gypsum: II. Effect of Sodium Hydroxide under Various Conditions, Journal of Chemical Technology and Biotechnology. 35 A (1985) 36–40. https://doi.org/10.1002/jctb.5040350107.

[72] R.M. Mota, A.S. Silva, V.H.S. Ramos, J.C.T. Rezende, E. de Jesus, Effects of storage temperature and time on false setting behavior of CPI-S Portland cement, Ceramica. 66 (2020) 321–329. https://doi.org/10.1590/0366-69132020663792842.